NISTIR 4443

SULFUR DIOXIDE CAPTURE IN THE COMBUSTION OF MIXTURES OF LIME, REFUSE-DERIVED FUEL, AND COAL

K. L. CHURNEY
T. J. BUCKLEY

U.S. DEPARTMENT OF ENERGY
Biofuels and Municipal Waste Technology Division
Office of Renewable Energy Technologies
1000 Independence Ave. S.W.
Washington, D.C. 20585

U.S. DEPARTMENT OF COMMERCE
Center for Chemical Technology
Chemical Thermodynamics Division
National Institute of Standards
and Technology
Gaithersburg, MD. 20899

U.S. DEPARTMENT OF COMMERCE
Robert A. Mosbacher, Secretary

NATIONAL INSTITUTE OF STANDARDS
AND TECHNOLOGY
John W. Lyons, Director

NIST

NISTIR 4443

SULFUR DIOXIDE CAPTURE IN THE COMBUSTION OF MIXTURES OF LIME, REFUSE-DERIVED FUEL, AND COAL

K. L. CHURNEY
T. J. BUCKLEY

U.S. DEPARTMENT OF ENERGY
Biofuels and Municipal Waste Technology Division
Office of Renewable Enery Technologies
1000 Independence Ave. S.W.
Washington, D.C. 20585

U.S. DEPARTMENT OF COMMERCE
Center for Chemical Technology
Chemical Thermodynamics Division
National Institute of Standards
and Technology
Gaithersburg, MD 20899

June 1990

Final Report for: DOE Interagency
Agreement No. DE-AI01-87CE31000 Mod. A002

Agreement Period: 2-8-89 to 5-1-90

U.S. DEPARTMENT OF COMMERCE
Robert A. Mosbacher, Secretary

NATIONAL INSTITUTE OF STANDARDS
AND TECHNOLOGY
John W. Lyons, Director

TABLE OF CONTENTS

1. Introduction

2. Summary of Results and Conclusions

3. Experimental Apparatus
   3.1 Description of the Combustor
   3.2 Modification of the Combustor

4. Experimental Procedures for the Sulfur and Chlorine Mass Balance Study
   4.1 Combustion Pellet Preparation
   4.2 Ash Preparation for Analysis
   4.3 Cleaning Procedures
   4.4 Analysis of Samples

5. Description of the Combustion Experiments

6. Chemical Analysis Results
   6.1 Initial Samples
   6.2 Chlorine Balance
   6.3 Sulfur Balance
   6.4 Calcium Balance and Calculated Ash Content

7. Combustion Results

8. Discussion and Applications

9. Conclusions

10. References

11. Appendices
   11.1 Uncertainty in the Total SO_2 in the Product Gas
   11.2 Formulae for Uncertainty in Total SO_2
      11.2.1 Stoichiometry
      11.2.2 Error Formula for SO_2
      11.2.3 Uncertainty in Total Inlet Oxidant Gas Flow Rate
      11.2.4 Uncertainty in Stoichiometry Correction
      11.2.5 Uncertainty in Water Vapor Correction
   11.3 Ash Computations
   11.4 Effective Ash Temperature
   11.5 Gas Thermocouples
      11.5.1 Introduction
      11.5.2 Model for the Regular Gas Thermocouple
      11.5.3 The Aspiration Experiment
      11.5.4 Model for the Aspiration Thermocouple (No Aspiration)
      11.5.5 Discussion

12. Acknowledgements

LIST OF TABLES

Table 1	Pellet Composition, Properties of Coal and RDF
Table 2	Chlorine Balance
Table 3	Sulfur Balance
Table 4	Calcium Balance
Table 5	Calculated versus Observed Ash
Table 6	Average Temperatures of Wall and Gas In Combustion Zone
Table 7	Model of Regular Thermocouple
Table 8	Model of Aspiration Thermocouple (No Aspiration Flow)
Table 9	Algebraic Formulae for Solutions to Regular Thermocouple Models
Table 10	Estimates of Radiation Corrections for Gas Thermocouples

LIST OF FIGURES

Figure 1 NIST Combustor

Figure 2 Sketch of Thermocouple and Oxidant Gas Nozzle Locations

Figure 3 Gas and Middle Wall Temperatures versus Time
Experiment 110 (7.1% lime, 0.2% MnO_2)

Figure 4 Combustor Wall, Ash Pan, and Baffle Temperatures versus Time
Experiment 110 (7.1% lime, 0.2% MnO_2)

Figure 5 Sample Surface and Gas Upper Side Temperatures, CO_2 and CO Prodution Rates versus Time
Experiment 110 (7.1% lime, 0.2% MnO_2)

Figure 6 Gas and Middle Wall Temperatures versus Time
Experiment 112 (3.5% lime, 0.0% MnO_2)

Figure 7 Combustor Wall and Baffle Temperatures versus Time
Experiment 112 (3.5% lime, 0.0% MnO_2)

Figure 8 Sample Surface, Upper and Lower Internal Sample, and Gas Upper Side Temperatures versus Time
Experiment 112 (3.5% lime, 0.0% MnO_2)

Figure 9 CO_2 and CO Production Rates, Oxygen Consumed/In, and Fraction Reacted versus Time
Experiment 112 (3.5% lime, 0.0% MnO_2)

Figure 10 Sulfur Dioxide Capture
SO_2 Capture, Ash Temperature, and CO_2 and CO Production Rates versus Time
Experiment 110 (7.1% lime, 0.2% MnO_2)

Figure 11 Sulfur Dioxide Capture
SO_2 Capture, Ash Temperature, and CO_2 and CO Production Rates versus Time
Experiment 112 (3.5% lime, 0.0% MnO_2)

Figure 12 Aspiration Experiment Results
Experiment 112 (3.5% lime, 0.0% MnO_2)

ABSTRACT

Chlorine and sulfur mass balance studies have been carried out in the combustion of mixtures of lime, refuse-derived fuel, and coal in the NIST multikilogram capacity batch combustor. The catalytic effect of manganese dioxide on the trapping of sulfur dioxide by lime was examined. Under our conditions, only 4% of the chlorine was trapped in the ash and no effect of manganese dioxide was observed. Between 42 and 14% of the total sulfur was trapped in the ash, depending upon the lime concentration. The effect of manganese dioxide on sulfur capture was not detectable. The temperature of the ash was estimated to be near 1200 °C, which was in agreement with that calculated from sulfur dioxide capture thermodynamics.

1. Introduction

The general aim of this study was to investigate whether or not coals containing sulfur in excess of two percent could be burned in an environmentally acceptable manner by co-firing the coal with refuse-derived fuel (RDF) containing a lime binder. The sulfur emission, SO_2 gas, which is formed in the combustion reaction is trapped in the ash residue by the reaction of the SO_2 gas with lime ($Ca(OH)_2$) and oxygen gas (O_2) to form $CaSO_4$. The lime is added to the input RDF and coal since it has been shown that lime is a suitable binder for enhancing RDF to environmentally acceptable, stable, and storable pellets of densified RDF (dRDF) that are similar to lignite coal [1].

The two specific objectives of the study were: to determine if catalysts can increase the trapping of SO_2 for mixtures of coal, RDF, and lime having a composition appropriate to real world incinerator conditions, and to characterize the combustion conditions in our combustor so that results might be applied to other methods of combustion.

To accomplish the first objective, manganese dioxide, MnO_2, was selected as the catalyst because the catalytic activity of MnO_2 in the trapping of SO_2 has already been demonstrated [2]. Manganese dioxide is commercially available as the mineral pyrolusite. We chose the ratio of the RDF to coal content for all experiments to be 30% on an enthalpy of combustion basis and the lime concentration for one pair of experiments (with and without catalyst) to be 3.5 mass percent. Assuming an enthalpy of combustion of 29.0 MJ/kg (12,500 BTU/lb) for coal and 15.1 MJ/kg (6,500 BTU/lb) for dRDF, a 3.5% lime content corresponds to mixing coal with dRDF having 8% lime binder. The RDF and lime concentrations are the maximum concentrations used in the co-firing tests run in a full-scale incinerator that were carried out by Argonne National Laboratory (ANL) and North Texas State University (NTSU) [3]. Our combustion samples were prepared from the same coal and RDF used in those co-firing tests.

To accomplish the second objective, additional temperature sensors were installed in our combustor to better characterize the temperature in the vicinity of the burning sample.

An idea of the upper limit of capture of sulfur under our combustion conditions was needed. Thus, the first pair of experiments carried out were two combustions of a mixture (with and without catalyst) of coal, RDF, and lime at a very high lime concentrations, 7.1%. The rationale for the selection of high lime concentrations and a high RDF/coal ratio was based on the following four considerations.

(1) An examination of thermodynamic data [4] shows that the temperature of the lime must be kept as low as possible while maintaining oxidative combustion conditions in order for the lime to trap significant amounts of SO_2.

(2) In our combustor, low temperatures normally correspond to reducing combustion conditions and high temperatures to oxidative conditions. This is a

consequence of the fact that the combustion sample is burned in the batch mode as a single pellet in flowing oxidant gas near atmospheric pressure. The rate of burning can be controlled only by the rate of supply and temperature of the oxidant gas and not also by the rate of supply of solid sample, as, for example, in an incinerator. To illustrate, in a previous experiment, we found that when a pellet consisting of a mixture of coal, RDF, and lime was burned under strongly oxidative conditions (i.e., the CO concentration in the product gas was <100 ppm) only a small amount of sulfur was trapped in the ash. This occurred not only because the lime content was low (actually 2% versus the nominal 4%) but probably also because the temperature of the lime in the ash was too high.

(3) However, combustion conditions for samples containing large amounts of lime are oxidative in our combustor although the temperatures of the combustor walls and the lime are low. Experiments carried out at NBS in 1988 [5] showed that when a pellet of RDF containing 7% lime or greater is burned, the combustor walls remain relatively cool, the lime/ash has the same form as the original pellet, and the CO_2/CO ratio is large during the main period of the burn and greater than one during the last part of the burn. We inferred from these observations that the average temperature of the lime remains low, the lime is in optimal position for trapping components of the product gas, and the combustion conditions where the sample is actually burning are strongly oxidative. We proposed that similar conditions ought to apply to a coal-RDF pellet containing 7% lime and to possibly to a lesser extent with 3.5% lime.

(4) The least energetic fuel should provide the lowest lime temperature and largest trapping capacity for sulfur and chlorine.The ratio of the RDF to coal content of 30% on a BTU basis was selected because this is the least energetic fuel used in the tests made in the summer of 1987 by NTSU at ANL.

Blank or reference experiments (e.g., coal alone, coal plus dRDF without lime, or dRDF alone) were carried out in earlier work in our combustor.

In the remainder of the text, we will refer to the pellets containing 7.1% lime and 3.5% lime as the high and low lime pellets or samples, respectively.

2. Summary of Results and Conclusions

The coal and lime contain 300 ppm and 150 ppm of chlorine, respectively, all in the form of water soluble chlorine, which we call chloride. The RDF contains an average of 0.38% total chlorine, of which 37% is chloride. The RDF is similar in total chlorine and chloride content to the RDF from Baltimore County examined in an earlier study [6]. The coal and RDF contained 2.9% and 0.31% sulfur, respectively.

Coal containing 3% sulfur cannot be burned in an environmentally acceptable manner in our combustor by co-firing the coal with RDF which contains lime as a binder. This is because the average temperature of the lime was too high, 1200-1300 °C. The temperature of burning and oxidative condition cannot be varied independently in our combustor to any significant extent. Approximately, 42% of the sulfur is trapped in the ash of the high lime

samples. For the low lime samples, the percentage of the sulfur trapped in the ash drops to 18-24%, when MnO_2 is present, and to 14-17%, when MnO_2 is absent. The moles of sulfur trapped in the ash divided by the moles of lime in the initial sample, the efficiency of capture, ranges from 0.23 to 0.29. The difference in trapping when MnO_2 is present or absent is not significant according to our uncertainty estimates.

Between 3% and 4% of the total chlorine in the sample is trapped in the ash of the high lime samples and less than 1% in that of the low lime samples. The effect of the presence or absence of MnO_2 on the trapping of chlorine in the ash could not be detected.

The bulk of the sulfur in the product gas is in the form of SO_2 gas. Only 7 to 23% of the sulfur in the product gas is lost as SO_3 gas and this percentage is not correlated with either lime concentration or the presence of MnO_2.

The temperature of the combustion flame is greater than 1800 °C. This is a consequence of the observation that one of the noble metal thermocouples used to monitor the temperature inside the sample pellet melted; the melting point is about 1800 °C. The pyrometer measurements of the temperature at the upper surface of the sample gave a lower bound of 1500 °C for the combustion flame temperature.

The gas mixture consisting of product gas, just after it leaves the pellet, and inlet oxidant gas, before it strikes or enters the pellet, has a nearly uniform temperature. The temperature is quite low, ~500 °C on the average, so the combustion reactions (e.g., conversion of CO to CO_2) are quenched once the product gases are a few centimeters away from the burning pellet. This is inferred from the close agreement of the temperatures registered by the noble metal gas thermocouples near the sample; the difference between the nominal and true gas temperature is estimated to be less than 50 °C.

The temperature of the lime in the ash is estimated from observations of temperatures inside and at the surface of the pellet to be near 1200 °C. This is close to the average temperature, 1200-1300 °C, predicted from thermodynamic considerations.

The maximum capture of SO_2 by lime can be predicted from thermodynamic considerations. Lower effective lime temperatures would increase the capture dramatically. For our method of combustion, this could probably only be accomplished by suspension of the lime above the combustion zone or, better, in a separate temperature-controlled lime scrubber downstream of the combustor. For methods of combustion that permit some degree of separate control of temperature of burning and oxidative condition, direct addition of lime would be more effective than in our combustor.

3. Experimental Apparatus

3.1 Description of the Combustor

The following is a shortened composite of the description given in reference [7] and modifications described in references [5], [8], and [9].

The study was carried out in the combustor of a multi-kilogram flow calorimeter [7] that was modified in later work so that the combustor and its enclosure could be operated in air [5]. A cross section of the apparatus is shown in figure 1. The combustion sample, A, is a compressed cylindrical pellet consisting of a mixture of coal, RDF, lime, and MnO_2. The pellet is supported on a horizontal lattice of nine alumina rods (6 mm in diameter) resting in notches cut in the top edge of a cup shaped ash pan, B. The ash pan catches the lime and the residual ash from the burned coal. The ash pan rests on the base access plate of the combustor, C. The sample is ignited by passing electrical current through an iron fuse wire connected between two vertical electrodes that are located on either side of the pellet. The electrodes pass through chimneys welded into the bottom of the ash pan. The electrodes as they appear above the ash pan and the iron wire having a coil touching the top center of the sample are shown in figure 1.

Oxidant gas is supplied to the sample through an array of five horizontal tiers of nozzles, J. The upper four tiers are shown as short lines perpendicular to the combustor wall in figure 1. Each tier has six symmetrically spaced nozzles located in the combustor wall. The lowest tier supplies a diffuse flow through slots in the ash pan to the underside of the sample. The upper tiers supply narrow jets of gas that are directed at the sides of the pellet or into the space above it.

The product gas flows upward through a 15 cm diameter port in the baffle, D, and out the cone-shaped top of the combustor through a tee with a window. The product gas then passes out and down an exhaust line to a ten turn cooling coil, K, and then to the water collector, L. The coil and collector are mounted in the water bath M which is kept near 11 °C. Water formed in the combustion drains from the upper, larger toroidal tube of the collector into the lower, smaller toroidal tube where it is not directly exposed to the flowing product gas. The product gas then leaves the collector and flows into the cold trap, N, and out the charcoal trap, P, into the laboratory exhaust. The cold trap is immersed in the cold bath, O, which is normally kept at or below -5 °C with an ethylene glycol, water, and dry ice mixture. For these experiments, the cold bath was removed; the cold trap was at room temperature.

The combustor, C, is mounted in a concentric cylindrical vessel, the combustor enclosure, F, which forms a pressure tight seal around the combustor which is operated at a positive pressure of 7-21 kPa (1-3 psig). Viton O-ring seals are maintained by cooling coils, I, and an annular water bath (not shown) on the top of the enclosure which protects the O-ring seals of the inlet oxidant gas supply tubes.

The oxidant gas is supplied to each tier of nozzles via a separate controller-flow meters in the oxidant gas supply manifold. Each inlet supply tube passes through the top of the combustor enclosure, F, into the space between the combustor enclosure and combustor to a three turn preheat coil welded to the outside of the combustor. The oxidant gas then passes through a single turn of tubing wrapped with a high temperature electrical heater and into a distribution ring tube which supplies the six nozzles of each tier.

The space between the enclosure and the combustor also contains electrical leads, alumina-silica insulation, E, around the lower part of the wall of the combustor, and a number of thermocouples. The thermocouples monitor the temperature of the oxidant gas as it enters each distribution ring, the baffle, nine locations on the combustor wall, and the product gas at the combustor exit.

A block diagram of the product gas analysis system is given in reference [7]; specification for these and other detectors and sensors are given in reference [9]. All measurements were recorded by an 80 channel computer controlled data logging system described in reference [9]. Each channel was read at least once per minute, converted to engineering units (temperatures, flow rates, gas concentrations, etc.), stored on a hard disk, displayed, and printed. The data were tabulated as a function of time and then exported through a serial port to a personal computer for analysis. Commercial spreadsheet and scientific analyses packages were used for most calculations.

3.2 Modification of the Combustor

To characterize the temperature around the burning sample, noble metal (type S and type B) thermocouples were installed to measure local gas temperatures near the side of the burning sample and a type K thermocouple was installed to monitor the product gas temperature in the port of the baffle. A radiation ratio thermometer, which we call the pyrometer, was mounted on the calorimeter lid above the viewing port in the tee of the gas exit of the combustor to monitor the temperature at the surface of the burning sample. The field of view of the pyrometer was centered on and had a diameter slightly less than that of the unburned combustion pellet (14.7 cm). The operating range of the pyrometer is from 650 to 1650 °C.

The noble metal gas thermocouples near the sample were mounted in twin-bore ceramic insulators supported at the side wall of the combustor. Because the gas velocity in the combustor is relatively low (e.g., the drift velocity of the product gas in the combustor is of the order of 7 cm/sec at 600 °C), the radiation correction to obtain the true gas temperature from the measured temperature could be substantial. To reduce the radiation correction, these thermocouples were made from small diameter wire (1/4 mm) and the thermocouple junction, which has a relatively low emissivity (estimated to be 0.1 to 0.2), was left bare. Calibration checks between runs were made to determine if a couple was damaged by exposure to the product gas. No changes in the thermocouples were detected. Since the radiation correction decreases as the velocity of the gas flowing past the thermocouple is increased, the thermocouple holder was designed to permit the option of aspirating the product gas past the thermocouple junction. Temperature measurements were made using the aspirated thermocouple in the last experiment and are discussed appendix 11.5.

In the last experiment, two type B thermocouple probes were inserted into radial holes drilled in the sample pellet 2.5 cm from its top and bottom to monitor the temperature of the ash (prior to its falling into the ash pan) and to obtain at least a lower bound to the combustion flame temperature.

4. Experimental Procedures for the Sulfur and Chlorine Mass Balance Study

4.1 Combustion Pellet Preparation

The sample pellet was prepared from high sulfur (~3%) Kentucky coal used in the NTSU/ANL incinerator tests, and from dRDF, also used in the incinerator tests, which had the NTSU/ANL designation MIN, 0% binder, no plastics. This particular dRDF was selected because it had been burned in previous work and had a relatively small chlorine content. Chlorine is a suspected "poison" for transition metal catalysts for uptake of SO_2 by lime[2]. The lime and MnO_2 were analytical reagents meeting ACS specifications.

The coal was manually fractured to -1 cm particle size and then milled to -1 mm particle size using a Brinkmann[a] ZM-1 mill. The dRDF was milled to 2 mm particle size using a Williams hammer mill followed by a Wiley mill; the milled dRDF is subsequently referred to as RDF. No dry ice was required to prevent the sample from overheating. The appropriate mass of RDF was homogenized in a large vee-blender. After a 100 g aliquot was removed for later analysis, the remaining mass of coal, lime, and MnO_2 were added and further homogenized. After removing a 100 g aliquot of the sample for later analysis, the remainder was pressed into a cohesive pellet using a pellet die of 14.6 cm (5.75 in.) in diameter and a force of 712 kN (160,000 lbf). Masses of materials added or removed from the blender were measured; the mass of material added to the blender always exceeded that removed by about 10 g. Loss by spilling or incomplete transfer does not account for this. The final pellet mass was between 2 and 2.2 kg. The combustion pellet was stored overnight in nested plastic bags and weighed a final time just before loading into the combustor. The dimensions of the pellets were 14.6 cm (5.75 in.) diameter and 12.7 cm (5 in.) in height except for experiment 109 where the height was 16.1 cm (6.34 in.).

The composition of the combustion pellets are given in the top of table 1 on an as-received basis. Since the results of previous combustions (runs 96-98) involving coal and RDF are cited in section 6, the composition of these pellets are also given in table 1, for convenience. The remainder of the data in this table are discussed in section 6.1.

4.2 Ash Preparation for Analysis

After the combustion experiment, the ash was examined (see section 5) and weighed. The ash pan with the ash was then stored, if necessary, in polyethylene bags - essentially no weight increase was observed over storage periods up to 48 hours even when the bags were open to the room air. The ash sample was reduced in particle size by grinding for 24 hours in a ball mill. This method was chosen over the ZM-1 mill used in some of the previous experiments reported in reference [5] because no sample is lost during the

---

[a] Certain facilities, commercial equipment, instruments, or materials are identified in this paper in order to adequately specify the experimental procedure. Such identification does not imply recommendation or endorsement by the National Institute of Standards and Technology, nor does it imply that the materials or equipment are necessarily the best available for the purpose.

grinding in the ball mill. The method had the drawback that portions of the ash that appeared fused were not completely reduced to powder in the ball mill, but remained as small hard nodules whose contents were not analyzed. Grab samples of the ash were used for laboratory analysis.

4.3 Cleaning Procedures

After dismantling the combustor and the product gas exit line, the collector with the condensate was weighed and the condensate was poured out and stored for later analysis. In experiment 109, no further analytical samples were prepared. In experiments 110-112, the collector and the glass wool filter in the exit port of the collector were washed in two changes of hot tap water (46 °C). This additional procedure was adopted to determine the error, if any, in the assumption that all chloride and sulfate are trapped in the condensate. After removal of the noble metal gas thermocouples from the combustor, the inside of the combustor, ten-turn cooling coil, cold trap, and connecting tubes between these units were also washed with hot tap water. The washings, amounting to some 64 kg of liquid, were collected in polyethylene buckets, weighed, and an aliquot of each bucket was removed for analysis. The precipitate in the washings in each bucket was concentrated by decantation of the supernatant liquid and combined in a large glass beaker. The composite slurry was acidified with concentrated HCl and then diluted to a final concentration of ~3N acid. An aliquot of this mixture was removed for later sulfate and calcium analysis. This procedure was adopted to determine if any $CaSO_4$, if present, had not dissolved in the condensate.

4.4 Analysis of Samples

Grab samples of the initial coal and RDF were analyzed for organic chlorine, inorganic chloride, total sulfur, residual moisture, and ash. The ash was analyzed for organic chlorine, water soluble chloride, and total sulfur. The RDF and the ash were also analyzed for calcium content. The ash from experiments 109 and 110, where the oxidant gas was turned off after 120 minutes whether the combustion was complete or not, was also analyzed for carbon and hydrogen by Leco Combustion. The condensate from the collector and the washings were analyzed for chloride, sulfate, and calcium. Organic chlorine was determined according to ASTM standard method D808. Water soluble chloride was determined according to ASTM E776-81 except that the titration method was EPA method 325.3 [10] and the analysis was performed on a filtered (0.45 micron) sample. Total sulfur was determined by ASTM standard method D129. Residual moisture was determined by ASTM standard method D2216, and ash was determined by ASTM standard method D482. Calcium was determined by EPA method 215.1 [10] with sample digestion according to EPA Method SW-846 [10]. Sulfate was determined by EPA method 375.4 [10] using a filtered sample (0.45 micron). The analyses were performed by Gascoyne Laboratories of Baltimore, Maryland.

5. Description of the Combustion Experiments

The combustor was flushed with air doped with oxygen to a final concentration of 50% oxygen for 15-20 minutes prior to ignition of the sample. About 4.5 minutes after ignition, the flow to the top tier of oxidant gas nozzles was

reduced or shut off and 30 minutes after ignition the flow to the #2 and #3 tiers of nozzles were shut off. When the flow to the top tier was turned off, the sample ceased to burn on its top surface as observed through the view port of the pyrometer.

The composition of the inlet oxidant gas during all the runs was held constant at 50±1 mol%. Typically, the initial flow rate was 285 slpm (standard conditions are 1 bar and 0 °C) with the bottom, top, #1, #2, and #3 tiers being supplied at a rate of 135, 70, 50, 15, and 15 slpm, respectively. The location of the various tiers in relation to the unburned pellet location is given in figure 2. The average total flow rate and combustor pressure for the duration of the burn was about 200 slpm and 10-25 kPa (1.5 to 3.5 psig), respectively.

After ignition, the CO production was quite low - less than 100 ppm. Thirty minutes or later after ignition the CO production began to rise slowly and finally peaked at about 0.1-0.2 mol% near the end of the burn. The temperatures of the combustor in the combustion zone (wall, ash pan, and baffle) peaked at 400-600 °C about 30-40 minutes after ignition. The temperatures of the gas at the side and above the pellet in the combustion zone varied with time in roughly the same way as the combustor but were greater by some 100-200 °C. The temperatures registered by the pyrometer consisted of an initial peak at ignition of 1200-1500 °C, then a decrease to a low temperature near 700 °C, followed by a broad plateau in the vicinity of 1000 °C. The plateau persisted until the end of the run for the high lime pellets and terminated (i.e., temperature fell below 650 °C) some 30 minutes prior to the end of the burn for the low lime pellets. Further description is given in section 6.

In experiments 109 and 110, the oxidant gas flow was turned off 120 minutes after ignition. This was done to eliminate appreciable sweeping off of the SO_2 captured earlier by the lime. When the CO_2 production is low, the SO_2 production is low and, thus, $CaSO_4$ will decompose to maintain the SO_2 equilibrium pressure, depending upon the local oxygen pressure and temperature of the solid $CaSO_4$. In the last two experiments the flow was kept on until the burning ceased as determined both visually and by the CO_2 and CO production. The combustion times for the last two runs were only slightly longer: 128 and 126 minutes for experiments 111, and 112, respectively.

The ash of the high lime pellets was similar to ash from pellets of RDF containing large amounts of lime obtained in previous experiments in that the ash resembled the shape of the original pellet. In experiment 109, part of the ash had fallen from the alumina lattice support; in experiments 110, the lime-ash structure remained intact on the support. The lime/ash was colored salmon pink on the outside; the color inside varied from brown near the outer surface to black bordering a hollow core. Generally the lime/ash in the earlier RDF-lime combustions was white to sand colored. The hollow core was considerably greater in size (on a proportional basis) than the size of the core observed in the RDF-lime combustions and also differed in having many rounded beads of ash on the surface of the core. The ash from the low lime pellets, experiments 111 and 112, had fallen into the ash pan but had the same variations in color noted above. Qualitatively, it seems clear that the appearance and structure

of the ash is consistent with the sample burning at a very high temperature inside a hollow core of the lime/ash which remains intact or disintegrates depending on whether the lime content is high or low, respectively.

6. Chemical Analysis Results

6.1 Initial Samples

The results of the analyses of the coal and RDF used in the pellets are given in the bottom of table 1. Analyses of the same coal and same RDF from three previous experiments, 96-98, carried out in 1988 are also given including some results of analyses carried out by a second analytical laboratory (Spots, Stevens, and McCoy). The moisture content of the coal seems to have decreased by about 0.5-1% over the two year period. The ash contents enclosed by parentheses are assumed ash contents. The lower moisture content of the RDF used in experiments 110 and 111 is probably due to grinding (Williams hammer mill and Wiley mill) of fresh dRDF.

6.2 Chlorine Balance

The results of the chlorine balance study are given in table 2. The first three rows (see numbers in the first column) give the total chlorine (the sum of the organic chlorine and chloride content) for the coal, RDF, and lime, respectively, in ppm and grams followed by the estimated uncertainty on an absolute basis in grams for each experiment. The last column on the right side of the table contains the uncertainty in ppm used to compute the absolute uncertainty for each measurement in the row. Rows 4 through 6 contain the chloride content of the coal, RDF, and lime. Analytical values for the lime are from the batch analysis of the analytical reagent used to prepare the sam ple. The average chlorine content of the coal and lime is 300 ppm and 150 ppm, respectively, and all the chlorine is in the form of chloride. The RDF contains an average of 0.38% total chlorine, of which 37% is chloride. The RDF is similar in total and water soluble chlorine content to the RDF from Baltimore County examined in earlier study [6].

The total chlorine in the sample in row 7 is the sum of rows 1 through 3 and the uncertainty is calculated as the sum of the absolute values of the individual uncertainties.

The chlorine in the combustion products is given in rows 8 through 11; total chlorine and chloride were determined for the ash; only chloride was determined for the condensate, given in row 10.

Using the data in the first eleven rows, one obtains the chlorine balance ratio, row 12, the fraction of the chlorine trapped in the ash, row 13, and the fraction of the chlorine in the ash that is chloride, row 14. The chlorine balance ratio equals one within the uncertainty estimates.

Only minimal trapping of chlorine occurs: 3-4% for the high lime concentration and 1% or less for the low lime concentration. All the trapped chlorine is in the form of chloride. The effect of the presence or absence of MnO_2 on the

trapping of chlorine in the ash is not significant according to the uncertainty estimates.

6.3 Sulfur Balance

The results of the sulfur balance are given in table 3. The quantities in the columns and the definition of uncertainties are the same as in table 2. Analytical values for the lime are taken from the batch analysis of impurities for the analytical reagent. Values for the total sulfur of coal, RDF, and lime are given in rows one through three and the total sulfur in the sample in row 4.

The total sulfur in the ash assuming the sulfur content of the ash is uniform is given in row 5 and assuming the hard nodules in the ash (i.e., that which could not be reduced to powder in the ball mill) contain no sulfur in row 6. The total sulfur in the condensate, analyzed as sulfate ion, is given in row 7. The values include the sulfate content of the precipitate in the washings that was acidified with hydrochloric acid in experiments 110 to 112. Row 8 contains the measured value of sulfur in the product gas in the form of SO_2 calculated from the absorbance of the product gas measured with the infrared trace component detector. The value is missing for experiment 109 because the input filter to the latter detector plugged during the experiment. Row 9 contains the calculated sulfur in the form of SO_2, assuming it equals the difference of the total sulfur in minus the sum of the sulfur in the ash and condensate. The total sulfur in the products, given in row 10, is the sum of rows 5, 7, and 8.

Using the data in the first ten rows, one obtains the seven ratios listed in rows 11 through 17. The sulfur balance ratio is given in row 11 and is discussed later. The fraction of the sulfur trapped in the ash based on the total sulfur in the products and based on the total sulfur in the initial sample is given in rows 12 and 13, respectively. The fraction of the sulfur in the product gas that is SO_2 gas and SO_3 gas, both based on the total sulfur in the products is given in rows 14 and 15, respectively. The SO_3 reacts with the water in the product gas to form H_2SO_4 which is collected in the condensate and washings.

We find that an average of 41% (from row 12) to 43% (from row 13) of the sulfur is trapped in the ash of the high lime samples. The percentage of the sulfur trapped in the ash of the low lime samples is 18-24%, when MnO_2 is present, and 14-17%, when MnO_2 is absent. The difference in the percentage of sulfur trapped in the ash in the presence and absence of the catalyst at both lime concentrations is not significant according to our uncertainty estimates, whether the basis is the total sulfur in or out.

From rows 14 and 15, we find that some 7 to 23% of the sulfur in the product gas is lost as SO_3 gas (calculated from the ratio of the value in row 14 divided by the sum of the values in row 14 and 15) and that the relative amount of SO_3 is not correlated with lime concentration or the presence of MnO_2. The bulk of the sulfur in the product gas is SO_2 gas.

The moles of sulfur trapped in the ash divided by the moles of lime in the initial sample, the efficiency of capture, is given in row 16. The efficiency is 0.24 when MnO^2 is present at either lime concentration. When MnO_2 is not present, the efficiency drops to 0.22 at the high lime concentration and 0.19 at the low lime concentration. For both the high and low lime concentrations, the difference in capture efficiency when MnO_2 is present or absent is not significant according to our uncertainty estimates.

The sulfur balance ratio, row 11, is equal to one within our uncertainty estimates because of the large uncertainty assigned to the SO_2 measurements. The reason for assigning a large error to the SO_2 measurements was that we could not account for the sulfur balance ratio on the basis of errors in the sulfur concentration in the coal or the ash. A large systematic error in the unburned coal can be ruled out on the basis that the sulfur content of the coal is relatively constant and two different analysts (Gascoyne Laboratories and Spots, Stevens, and McCoy) obtain the same values within the uncertainty estimates. A large systematic error in the sulfur content of the ash seems equally unlikely. The systematic error in the sulfur content of the ash for experiments 111 and 112 would have to be equal to the entire sulfur content of the ash or more, which is unreasonably large. Accordingly, we concluded that the measured values of SO_2 given in row 17 are, on the average, too large by 23% and set the uncertainty equal to 23%. This uncertainty estimate is larger than the estimate based on considerations other than the sulfur balance ratio. This estimate and further comments are given in section 11.1.

6.4 Calcium Balance and Calculated Ash Content

The results of the calcium analyses are given in table 4. The calcium in the coal was not measured and is assumed to be negligible. The total calcium in the lime is computed on the basis of our impurity analysis for this analytical reagent. The data of row 6 show that significant amounts of calcium were present in the condensate or washings in only experiment 112, in which one of the thermocouples was aspirated. Presumably aspiration tended to scatter and entrain more ash in the product gas.

The calcium balance ratio, given in row 8, is equal to one within our uncertainty estimates only for experiment 111. We concluded that calcium escaped past the cold trap shown in figure 1. This is consistent with the observed tendency of filters in the analysis and product gas exit line to plug.

The amount of ash expected was calculated and compared to the ash actually observed to see if this difference was consistent with the calcium loss in table 4. The results are given in table 5. The first four rows are the assumed ash content of the coal (except the measured value for experiment 112), the measured ash content of the RDF, the mass of MnO_2, and the mass of lime.

The increase in mass associated with the formation of $CaSO_4$ with the remainder present as lime is given in rows 5. The values are calculated from the measured sulfur content of the ash in table 3, as summarized in appendix 11.2. The calculated ash content corresponding to row 5 is given in row 7. The calculated mass of ash is about 10% larger than the observed ash.

The increase in mass associated with the formation of $CaSO_4$ and the corresponding calculated ash assuming that all that calcium in the initial sample that is not in the ash is due to loss of lime are given in rows 6 and 8, respectively. The values of row 8 are 5% larger, on the average, than the observed ash. The better agreement of the values in row 8, as compared to row 7, with the observed ash supports the idea that the calcium loss indicated in table 4 is genuine.

Correction of the sulfur capture efficiencies given in row 16 of table 3 using the calcium balance ratios given in row 8 of table 4 gives values of 0.28±0.03, 0.29±0.02, 0.26±0.03, and 0.23±0.03 for experiments 109, 110, 111, and 112, respectively. These values are on the average 20% larger than the values of row 16 table 3. Their large uncertainty obscures any difference between the presence and absence of MnO_2 or the difference between high and low lime samples.

7. Combustion Results

The gas temperatures at the side and just above the combustion pellet are shown in figure 3 for experiment 110 (7.1% lime, 0.2% MnO_2) as a function of time along with the middle wall combustor temperature for reference. The second lower side gas temperature is not shown since it lies within 10-20 °C of the first lower side gas temperature. The exact location of the thermocouples is given in figure 2. The combustor wall and ash pan temperatures are given in figure 4 as function of time for the same experiment. The location of these thermocouples are also given in figure 2. The temperature indicated by the pyrometer is given in figure 5 along with the upper side gas temperature for reference. (The low end of the pyrometer range is 650 °C.) The rise in the pyrometer temperature (curve A) near the end of experiment 110 at 200 to 210 minutes corresponds to a fracture in the top of lime/ash structure and the appearance of flame in the center of the pellet as observed through the view port of the pyrometer.

The rate of production of CO_2 (curve C) is given in figure 5 to indicate the heat release as a function of time. The CO_2 production is largest shortly after ignition, falls, then builds up again at 125 minutes, and then decays smoothly until it again begins to increase at 170-180 minutes. The third peak in the CO_2 production just precedes the appearance of flame on the top of the pellet.

As mentioned in section 5 and as shown in figure 5, the CO production (curve D) is quite low, ~100 ppm (in the dry product gas), after a small peak just after ignition. About 40 minutes after ignition, the CO concentration started to increase slowly and reached a maximum of ~0.1% about 100 minutes after ignition. This broad second peak in the CO production, called burnout, is about 90 minutes in duration. The CO_2/CO ratio remains greater than one throughout the experiment. In experiments with pellets of RDF alone, the duration of burnout is about 45 minutes and the CO_2/CO ratio falls below one during burnout. In experiments with pellets of RDF containing $\geq$7% lime, burnout at the end of combustion does not occur and the CO_2/CO ratio remains greater than one throughout the experiment.

The corresponding temperature-time relations for the various thermocouples and the pyrometer for experiment 112 (3.5% lime, no MnO_2) are given in figures 6, 7, and 8. The temperature-time behavior of the gas and combustor temperatures in figures 6 and 7, respectively, are similar to those of figures 3 and 4 except that the temperature peaks before the final decay at the end of the experiment are more pronounced and occur sooner after ignition in the low lime pellets.

Figure 8 gives the pyrometer temperature, the temperatures at points initially 2.5 cm within the surface of the pellet at heights 2.5 cm below the top and 2.5 cm above the bottom of the initial pellet, and the upper side gas temperature. The upper and lower internal pellet temperatures (curves B and C, respectively) rise in concert from ignition to a temperature some 100 to 200 °C above the pyrometer temperature (curve A) at 90 minutes, which is consistent with the sample burning from its outer surface inward. The upper pellet thermocouple evidently melted at this point, thus, setting a lower bound on the combustion flame temperature of 1800 °C.

Between 90 and 110 minutes, the temperature registered by the lower pellet thermocouple changes with time in the same way as the pyrometer temperature but remains about 100 °C greater than the pyrometer temperature. This suggests the temperature of the ash immediately adjacent to the combustion flame is of the order of 900 to 1100 °C.

The decay of the temperature indicated by the lower pellet thermocouple between 110 and 130 minutes, even though the pyrometer temperature continues to remain between 1000-1400 °C, suggests the ash and burning sample have fallen away from the lower pellet thermocouple. This is consistent with the visual observation that the burning sample was falling off the supporting lattice into the ash pan during this time interval.

The CO_2 and CO production rates for experiment 112 are given in figure 9 in curves A and D, respectively. The CO_2 production rate shows a much more pronounced peak than for experiment 110; the peak exceeds the level at ignition. This would be consistent with the lime/ash framework starting to break up and fall along with burning sample into the ash pan for the low lime pellets. The peak just precedes the rise in the pyrometer temperature, a feature also observed for the high lime pellets. At 110 minutes, some 25% of the sample is still unburned, according to curve C of figure 9. The oxygen consumption has risen from 1/3 to 1/2 of the inlet oxygen flow rate according to curve B. The CO production, curve D, differs from that for the high lime pellets in that the production is smaller (20-100 ppm) and remains so for a longer time after ignition. The final peak is much sharper.

The average temperatures for the thermocouples in the combustion zone and the pyrometer are given in table 6. Averages are for the duration of each experiment for thermocouples and for the time during which the pyrometer is in range. (i.e., when it is "on"). The thermocouple and pyrometer data suggest the product gas, just after it leaves the pellet, and the inlet oxidant gas, before it strikes or enters the pellet, constitute a mixture having a nearly uniform temperature. The temperature is quite low, ~500 °C on the average, so

the combustion reactions (e.g., conversion of CO to CO_2) are quenched once the product gases are a few centimeters away from the burning pellet. Mixing and stirring is accomplished by the jets of incoming oxidant gas (i.e., not by turbulent flow, per se). The product gas is cooled further by heat exchange with the combustor walls, ash pan, and baffle. The pyrometer data along with visual observations through the view port of the pyrometer indicate that the temperature in the actual combustion zone is in excess of 1500 °C; the pellet thermocouple sets a lower bound of 1800 °C.

The temperatures registered by the gas thermocouples located near the sample are estimated to be within 50 °C of the actual gas temperature. Estimates of error and analysis of the aspiration experiment carried out during run 112 are given in appendix 11.5.

The key to prediction of the trapping capacity of the lime for SO_2 is the average temperature of the lime exposed to the product gas. Data obtained with the lower pellet thermocouple suggest the temperature of the ash is in the vicinity of 900-1100 °C. To check this estimate, we have calculated the temperature of the $CaSO_4$ which is formed by capture of SO_2 gas by the lime, assuming it is in equilibrium with its decomposition products: quick lime (CaO), O_2 gas, and SO_2 gas. The reaction and the associated equilibrium constant, K, are:

$$CaSO_4(s) = CaO(s) + SO_2(g) + (1/2)\,O_2(g) \qquad (1a)$$

$$K_{eq} = P_{SO2}[P_{O2}]^{.5} \qquad (1b)$$

The equilibrium constant data of Stern et. al.[4] were fitted as a function of absolute temperature, T_{eq}, between 700 K and 1800 K to obtain the following expression;

$$\ln K_{eq} = 30.83909 - 57701/T_{eq} \quad , T_{eq} \text{ in K} \qquad (2)$$

Temperatures calculated with values of K_{eq} and equation 2 are within 10 K of the "known" temperatures from 300 to 1600 K. The pressures of SO_2 and O_2 in the combustion zone were calculated from the total pressure in the combustor and the mole fraction of these species as described in Appendix 11.4.

Plots of T_{eq} calculated from equation 2 are given in figures 10 and 11 for experiments 110 and 112, respectively. The rate of production of CO_2 and CO is given in each figure to indicate there is a rise in T_{eq} corresponding to the "second" peak in CO_2 production and the temperature drops off when the CO production ceases at the end of "burnout". The uncertainty in T_{eq} is estimated to be 30 °C. The average temperature over the duration of experiments 110, 111, and 112 were 1216, 1201, and 1287 °C, respectively. These temperatures are somewhat higher but are still relatively close to the ash temperature indicated by the lower pellet thermocouple. The average ash temperature might be lower than these values if the time of exposure and/or other conditions are insufficient for equilibrium. With this in mind, the average values of T_{eq} can be called the effective average ash temperature. The importance of temperature is reemphasized by examining the rate of capture of SO_2 as a function of time as shown in curve C of both figures 10 and 11. The method of computation is

given in appendix 11.4. A rise of about 30 °C in T_{eq} near the end of each run forces the capture rate to go negative - the $CaSO_4$ starts to dissociate.

8. Discussion and Applications

As noted before, in order to burn the combustible fraction of a solid sample as completely as possible to carbon dioxide and water in the batch mode, the solid sample must be burned as a pellet in order to restrict the rate of combustion of the sample. The oxidative condition and temperature of burning cannot be controlled independently. In the previous section, we have constructed a picture of how the pellet actually burns and have concluded that the effective average ash temperature is of the order of 1200 °C in our experiments. This is the reason the SO_2 capture by the lime is small, between 0.2-0.3 moles of sulfur per mole of lime.

The capture of SO_2, whether expressed on the basis of per mole of lime added or percentage of the total sulfur in the combustion products is the same, for practical purposes, whether manganese dioxide is present or not. Either the actual ash temperature was high enough to ensure equilibrium or the effect of manganese dioxide was blocked by conditions that automatically eliminate achievement of equilibrium conditions. One condition might be insufficient exposure time of the lime to product gas. Another condition might be physical impediment of the volume expansion of CaO for formation $CaSO_4$ [2].

Lower effective lime temperatures would increase the capture dramatically because of the exponential dependence of K_{eq} on T_{eq}. For our method of combustion, suspension of the lime above the combustion zone or, better, in a separate temperature-controlled lime scrubber downstream of the combustor would be the method of choice. For methods of combustion that permit some degree of separate control of temperature of burning and oxidative condition, direct addition of lime would be more effective than in our combustor. Under these circumstances, MnO_2 may be needed as catalyst for SO_2 capture. An additional question, which our experiments did not address, would then be prevention of the poisoning of the catalyst.

9. Conclusions

Coal containing 3% sulfur cannot be burned in an environmentally acceptable manner in our combustor by co-firing the coal with RDF which contains lime as a binder. This is because the average temperature of the lime was too high, 1200-1300 °C. The temperature of burning and oxidative condition cannot be varied independently in our combustor to any significant extent.

The percent of sulfur trapped in the ash was 42 % and 14-24% for samples having an initial overall concentration of 7.1% and 3.5% lime, respectively. The moles of sulfur trapped in the ash divided by the moles of lime in the initial sample, the efficiency of capture, ranges from 0.23 to 0.29. The difference in either the percentage or efficiency of trapping when MnO_2 is present or absent is not significant according to our uncertainty estimates.

Less than 4% of the total chlorine is trapped in the ash and the effect of the presence of MnO_2 on the chlorine trapping could not be detected.

The combustion conditions have been characterized as follows:

The temperature of the combustion flame is greater than 1800 °C.

The product gas just after it leaves the pellet and the inlet oxidant gas before it strikes or enters the pellet constitute a mixture having a nearly uniform, low, temperature. Combustion reactions (e.g., conversion of CO to CO_2) are quenched shortly after the product gases are a few centimeters away from the burning pellet.

The temperature of the lime in the ash is estimated from observations of temperatures inside the pellet to be near 1200 °C. This is close to the average temperature, 1200-1300 °C, predicted from thermodynamic considerations.

From the combustion results, we conclude that maximum capture of SO_2 by lime can be predicted from thermodynamic considerations.

10. References

[1] Daugherty, K.E., Safa, A., Ohlsson, O.O., and Venables, B.J., Proceedings of the American Power Conference 48, 930 (1986).

[2] Dr. Allen Van Till, U O P Reasearch Center, Des Plaines, IL, private communication, 1989.

[3] Ohlsson, O.O., Venables, B.J., and Daugherty, K.E., "Draft Test Plan for Determining the Combustion Performance and Impact of Cofiring Pelletized dRDF/Coal Blends on Plant Operation and Emissions", Argonne National Laboratory, Energy and Environmental Systems Division, Argonne, Illinois.

[4] Stern, K.H., and Weise, E.L., "High Temperature Properties and Decomposition of Inorganic Salts, Part I. Sulfates" NBSRDS-NBS 7, National Standard Data Series - National Bureau of Standards 7 October 1, 1966, Superintendent of Documents, U.S. Government Printing Office, Washington D.C., 20402.

[5] Churney, K.L., Ledford, A.E., Jr., Buckley, T.J., and Domalski, E.S., "Chlorine Mass Balance in the Combustion of Refuse-Derived Fuel", Proceedings of the 1988 National Waste Processing Conference, May 1-4, 1988, Philadelphia, Pennsylvania, page 47, The American society of Mechanical Engineers, United Engineering Center, 345 East 47th Street, New York, N.Y., 10017

[6] Domalski, E.S., Churney, K.L., Ledford, A.E., Jr., and Bruce, S.S., "Monitoring the Fate of Chlorine from MSW sampling through Combustion. Part I: Analysis of Sample Waste Stream for Chlorine", Chemosphere 15, 1355 (1986).

[7] Churney, K.L., Ledford, A.E., Reilly, M.J., and Domalski, E.S., "A Multikilogram Capacity Calorimeter for Heterogeneous Materials", Journal of Research of the National Bureau of Standards 91, 277 (1986).

[8] Domalski, E.S., Churney, K.L., Ledford, A.E., Jr., Bruce, S.S., Buckley, T.J., Parris, R.M., and Chesler, S.N., "Monitoring the Fate of Chlorine from MSW sampling through Combustion. Part II: Combustion Studies", Chemosphere 15, 1355 (1986).

[9] Buckley, T.J., and Rukkers, J.M., "A Computer Controlled Data Acquisition System for Combustion Calorimetric Experiments", Journal of Research of the National Bureau of Standards 93, 145 (1988).

[10] Kopp, J.F. and McKee, G.D., "Methods of Chemical Analysis for Water and Wastes. Third Edition. EPA Report No.: EPA-600/4-79-020. NTIS order no. PB84-128677. Springfield VA: U.S. Department of Commerce, National Technical Information Service, March 1983.

11. Appendix

11.1 Uncertainty in the Total SO_2 in the Product Gas

The total SO_2 in the product gas was determined by monitoring the optical absorbance of the product gas at the point where it leaves the cold trap. The absorbance is measured at 1160 cm^{-1} in a 20.25 m path length gas cell using a microprocessor controlled single beam infrared detector. The cell is held at a constant temperature of ~80 °C. The absorbance and the pressure at the outlet of the instrument are measured as a function of time and the mole fraction of SO_2 in the product gas is calculated as a function of time from a calibration equation. The total moles of SO_2 is calculated by multiplying the mole fraction of SO_2 by the molar flow rate of the product gas at the exit of the cold trap, called the moist product gas, to obtain the molar flow rate of SO_2 and then integrating the later over the duration of the combustion experiment.

The molar flow rate of the moist product gas is calculated from the total inlet oxidant gas flow rate and two corrections. The first, called the stoichiometry correction, accounts for the difference in molar flow rate of the inlet oxidant and dry outlet product gas at the exit of the cold trap. The second correction, called the moisture correction, is the adjustment to the dry product gas flow rate for the presence of a small amount of water vapor in the product gas. Formulae for the corrections and the basis for estimates of error in the flow rate of the moist product gas are given in appendix 11.2.

The calibration equation was determined with SO_2 at 0.106 mol% in N_2 obtained from Matheson Co. and at 0.261 mol% in N_2 supplied by the Gas and Particulate Division of NIST. The concentration of each mixture was determined by Dr. Gerald Mitchell of the NIST Gas and Particulate Science Division using a fluorescence technique. Our detector was calibrated by measuring the optical absorbance as a function of total pressure at the detector from 13 kPa (100 torr) to 106 kPa (800 torr) under static conditions for each mixture. The data were fitted by least squares with an equation expressing the partial pressure of SO_2 as a function of absorbance. The equation fits the two sets of data with a standard deviation of 2.0 Pa (0.015 torr); the maximum difference between calculated and observed partial pressures of SO_2 is 2.2 Pa (0.017 torr). The error in the mole fraction of SO_2 calculated from the calibration equation was estimated to be a constant value of 4.3×10^{-5}. The effects of pressure broadening by non absorbers are believed to be within this uncertainty. The correction of the static measurements to flow conditions, since the product gas is sampled at a rate of 5 slpm, was checked and found to be well within the preceding uncertainty limits. The instrument gain for experiments 110 to 112 was the same.

The uncertainty in the total SO_2 measurements are estimated separately for the high and low lime pellets since the average mole fraction of SO_2 over the duration of an experiment is 4.8×10^{-4} for the low lime and 7.7×10^{-4} for the high lime experiments.

Error Source	Percent Uncertainty in total SO_2 High lime	Low lime
Calibration equation	6	9
Flow rate of product gas		
Total inlet oxidant gas flow rate	10	10
Stoichiometry correction	0.4	0.4
Water vapor correction	0.1	0.1
Total	12-16	13-20

The smaller of the total uncertainty estimates is the square root of the sum of the squares; the larger is the sum of the separate errors. The above estimates of error are a factor of 0.5 to 0.8 times the 23% reduction in the values of the total SO_2 required to make the sulfur balance ratios for the experiments equal to one.

Sulfur balance tables (similar to table 4) for earlier experiments involving coal were recalculated using the new calibration data and method described above for the determination of SO_2 in place of the earlier assumption that the sulfur balance ratio is one and calculating the total SO_2 by difference. The earlier experiments were: a) coal with cellulose, experiment 96; b) coal plus RDF of the type used in experiments 109 to 112, experiment 97, and c) coal plus RFD having a 2% lime binder, experiment 98. The recalculated sulfur balance ratios for experiments 96, 97, and 98 are 0.97, 1.16, and 1.00, respectively. The gain of the SO_2 detector was not recorded for those experiments so the preceding sulfur balance ratios are uncertain in this regard to about 10%. (Sector gains of the instrument have been constant to about this extent throughout the work.) None of the results are between 0.8 and 0.7 as in the current experiments. A possible explanation may be that other gaseous species are absorbing at the 1160 cm^{-1} setting for our detector in the current experiments and this causes the nominal SO_2 to be large. It is pertinent that we have not run an infrared spectrum of the product gas for a coal combustion.

11.2 Formulae for the Uncertainty in the Total SO_2

11.2.1 Stoichiometry

The flow rate of the dry product gas at exit of the cold trap is calculated from the input flow rate, assuming that the rate of any reaction or process that causes a change in the total moles of gas, except the reaction for production of CO, is proportional to the rate of production of carbon in the products. The latter rate is assumed to be the sum of the molar rates of production of CO_2 and CO. The constant of proportionality is assumed to be independent of time and given by the overall reaction stoichiometry. The error in the assumption is small when: (1) the rate and total amount of hydrocarbons of variable and/or unknown composition that are produced is negligibly small and (2) the change in moles produced by relevant reaction or processes that fail to meet this assumption is small.

Some bookkeeping shows that, with the above assumption, the dry product gas molar flow rate, $N_{out}(dry)$, is given by:

$$N_{out}(dry) = N_{in}/[1-Z] \qquad (11\text{-}1)$$

where N_{in} is the total inlet oxidant gas molar flow rate and Z is the stoichiometry correction cited in appendix 11.1. This correction is given by:

$$Z = [Z_0(X_{CO}+X_{CO2}) + X_{CO}/2] \qquad (11\text{-}2)$$

$$Z_0 = -b/4a + c/2a - 3d"/2a + e/2a + f/4a \qquad (11\text{-}3)$$

where X_{CO} and X_{CO2} are the mole fractions of CO and CO_2 in the dry product gas. The parameters a,b,c,d", e and f are parameters in the combustion reaction which is written in the form:

$$n_0O_2(g) + mC_aH_bO_cS_dN_eCl_fgH_2O(r)(s) = (ma-1)CO_2(g) + (mb/2-mf/2+g)H_2O(g)$$

$$+ (1)CO(g) +(md')SO_2(g) + (md")SO_3(g) + (me/2)N_2(g) + (mf)HCl(g) \qquad (11\text{-}4)$$

where $$d = d'+d" \qquad (11\text{-}5)$$

$$n_0 = m(a + b/4 - c/2 + d'+ 3d"/2 - f/4) - 1/2 \qquad (11\text{-}6)$$

In this last equation, (g) indicates a gas and (s) a solid. The parameter n_0 is the moles of oxygen that react with the solid combustion pellet containing m formula weights of a combustible fraction that has the formula $C_aH_bO_cS_dN_eCl_f$. The m formula weights are associated with g moles of residual moisture which is designated $gH_2O(r)$.

The CO_2 and the CO are measured in dry product gas to eliminate the change in zero offset of the infrared detectors that would be caused by scattering of light in the infrared by droplets of condensed water. Thus, the molar flow rates of CO_2 and CO, N_{CO2} and N_{CO}, are given by:

$$N_{CO2} = X_{CO2}N_{in}/[1-Z] \qquad (11\text{-}7)$$

$$N_{CO} = X_{CO}N_{in}/[1-Z] \qquad (11\text{-}8)$$

The total output flow rate from the cold trap differs from the dry product gas in containing the mole fraction X_{WV} of water vapor. The total flow rate of the moist product gas, $N_{out}(moist)$, is given by:

$$N_{out}(moist) = N_{out}(dry)/[1-X_{WV}] \qquad (11\text{-}9)$$

where X_{WV} is the water correction cited in appendix 11.1. Thus, the molar output flow rates of water vapor, N_{WV}, and SO_2 gas, N_{SO2}, are given by:

$$N_{WV} = X_{WV}N_{in}/[(1-X_{WV})(1-Z)] \qquad (11\text{-}10)$$

$$N_{SO2} = X_{SO2}N_{in}/[(1-X_{WV})(1-Z)] \qquad (11\text{-}11)$$

where X_{SO2} is the mole fraction of SO_2 in the moist product gas. Both X_{WV} and X_{SO2} are monitored in the moist product gas.

In equation (11-4), the value of ma is the total moles of carbon dioxide and monoxide in the product gas, the sum of the integrals over the burn time of equations (11-7) and (11-8). The value of mb is calculated from the total moles of water formed:

$$\text{Moles of water formed} = mb/2 - mf/2$$
$$= (COL+CT+n_{WV} - md"[SO_3] - mf[HCl] - RM)/[H_2O] \qquad (11\text{-}12)$$

In equation (11-12), COL and CT are the increase in mass of the collector and cold trap, respectively. The parameter n_{WV} is the integral of equation 11-10 and RM is the residual moisture in the sample. Quantities in the brackets [] stand for the molecular weight of the corresponding species. In equation (11-4), the value for md' is the total moles of sulfur dioxide gas, the integral of equation (11-11). The value of md" is the total moles of sulfate in the products, the value of me is the total moles of nitrogen in the components of the initial sample, and mf is the total moles of chlorine in the products. The value of mc is calculated by difference using the other stoichiometry coefficients and the moisture and ash free masses of the coal and RDF:

$$mc = (TM - RM - ASH - ma*[C] - mb*[H] - md*[S] - me*[N] - mf*[Cl])/[O] \qquad (11\text{-}13)$$

where TM is the total mass in grams of the initial pellet, RM is the total mass of residual moisture, and ASH is the ash from the pellet assuming the lime does not change mass. Quantities in the brackets [] stand for the molecular weight of the corresponding species. The sulfur in the ash, condensate and washings of the combustor, traps, and flow lines are treated as sulfate. The values of md", me, and mf were determined from separate analyses by our analyst, Gascoyne Laboratories. Using these values, the values of ma, the fraction of mb due to the water vapor lost from the combustor, mc, and md' were determined iteratively from the monitored, CO_2, CO, water vapor, and SO_2 in the product gas. Only one or two iterations are needed to obtain results that are consistent within their uncertainties.

The stoichiometry correction factor, Z, contains no terms for the production of CO_2 and SO_2, since these reactions do not alter the total flow rate. The terms are for the reactions which produce CO, H_2O, SO_3, N_2, and HCl. The last four reactions are accounted for in Z_0, equation (11-3), and arise as follows. The production of water involves only the consumption of O_2 at a rate proportional to [(mb-mf)/4 - mc/2] since no water is present in the dry product gas. The production of SO_3 involves the consumption of oxygen at a rate proportional to 3md"/2 since it is assumed all SO_3 reacts with water to remain in the collector or cold trap or is trapped in the lime according to reaction (1a) of the text. Nitrogen is produced at a rate proportional to me. The production of HCl involves no correction since we assume all HCl is trapped in the condensate.

For combustion of a CHO organic, when no CO is formed, Z_0 is negative when b>c/2 since O_2 must be consumed to oxidize the H and O in the pellet to H_2O. In this case, N_{out}(dry) is < N_{in}. If b equals c/2 as it does in cellulose, and nearly so in the case of RDF, then -b/4a+c/2a is nearly zero and N_{in} ~ N_{out}(dry).

The magnitude of Z_0 in equation (11-3) ranged from -0.12 to -0.14 for the four experiments carried out in this study. Since the mean value of $X_{CO} + X_{CO2}$ for an experiment is about 0.1, the total outlet molar flow rate, N_{out}(dry), is 98.7% of the total input oxidant gas flow rate. The mean value for the mole fraction of water vapor in the product gas leaving the cold trap is 1 mol%, so the net correction for stoichiometry and water vapor is 0.3%.

11.2.2 Error formula for SO_2

The integral of equation (11-11) over the total burn time yields the total moles of SO_2, n_{SO2}. Since N_{in} is constant and X_{WV} and Z are small in comparison to one, the fractional error in the total moles of SO_2, dn_{SO2}/n_{SO2}, was estimated from:

$$dn_{SO2}/n_{SO2} \sim dX_{SO2}/X_{SO2} + (dN_{in}/N_{in} + dX_{WV} + dZ)$$

where dX_{SO2}, dN_{in}, dX_{WV}, and dZ are the the absolute value of the uncertainty in the average of X_{SO2}, N_{in}, X_{WV}, and Z, respectively. The sum of the quantities in the brackets () is the fractional error in the average flow rate of the product gas.

11.2.3 Uncertainty in the Total Inlet Oxidant Gas Flow Rate

The inlet oxidant gas flow meters are calibrated by intercomparing the various flow meters with respect to each other and then calibrating one or more of the meters on an absolute basis. The ratios of total flow rates of the individual flow meters were checked and found to be the same (within 2%) as those when two of the flowmeters were last calibrated. Since one of the flow meters has not been calibrated recently, the uncertainty in the total flow rate was increased from 5% at the last calibration [6] to 10%. Thus, dN_{in}/N_{in} = 10%.

11.2.4 Uncertainty in the Stoichiometry Correction

Since the mean value of X_{CO} is less than 1% of the mean value of X_{CO2}, and Z_0 is about 0.1, Z is given by

$$Z \sim (-mb/4 + mc/2 - 3md''/2 + me/2 + mf/4)(X_{CO2}/ma)$$

The parameter having the largest uncertainty in this expression is the CO_2 concentration. The CO_2 concentration is measured by determining the absorbance as a function of time of the moist product gas that has been dried. The non dispersive infrared detector was calibrated under static conditions with 10, 20, 35, and 50 mol% CO_2 in O_2. A correction is applied to convert from static to flow conditions. The coefficients in the calibration equation are corrected for each "unknown" measurement to the actual total pressure at the detector using pressure factors determined in the calibration. The uncertainty in X_{CO2}

was set at 10% (constant over the range) because the detection system was found to be operating improperly after the experiments had been completed.

Using equation (11-13), one has from the preceding formula:

$$dZ-(X_{CO2}/ma)*d(mc)/2=X_{CO2}*([C]/[O])*(d(ma)/ma)/2$$
$$-X_{CO2}*([C]/[O])*(dX_{CO2}/X_{CO2})/2$$
$$=0.1*12/16*10\%/2 = 0.38\%$$

11.2.5 Uncertainty in Water Vapor Correction

The mole fraction of water was determined by measuring the absorbance at ~1540 cm^{-1} (nominal instrument setting) of the moist product gas using the microprocessor controlled infrared detector used to monitor SO_2. A component of the product gas having a higher dew point than water interferes with the dew point meter that is ordinarily used for this purpose. The detector was calibrated by comparison of absorbance with the mole fraction of water for earlier experiments where the dew point meter was operating properly. The uncertainty in the mole fraction of water vapor is estimated to be 0.1 of the mean value. Thus, $dX_{WV} = 0.1* 1\% = 0.1\%$.

11.3 Ash Computations

To account for the formation of $CaSO_4$ in the calculated ash, the mass percent sulfur in the ash, %S, is expressed in terms of the moles, y, of $CaSO_4$ formed as given by:

$$\%S/100= y*AW(S)/[x*AW(lime)+ y*AW(CaSO_4)+ ash(coal)+ ash(RDF)+ MnO_2] \quad (11\text{-}12)$$

In equation (11-12), x is the moles of unreacted lime, AW stands for atomic weight of the species in parentheses, and ash is the mass of ash contributed by the component of the initial sample enclosed in parentheses, and MnO_2 is the mass of the catalyst in the sample. Taking advantage of the fact that

$$(x+y)*AW(lime) = lime$$

where lime is the mass of lime added to the initial sample, one can rewrite equation (11-12) in the form:

$$\%S/100 = y*AW(S)/[y*(AW(CaSO_4)-AW(lime)) + Ash]$$

where Ash is the sum of the ash contributed by each component of the initial sample separately without any formation of $CaSO_4$ (or lime loss, etc.). The mass change to be added to ash is given by:

$$CaSO_4 \text{ form.} = y*(AW(CaSO_4)-AW(lime))$$
$$= Ash*\%S/100*62.0428/[32.06-62.0428*\%S/100]$$

where 32.06 is AW(S) and 62.0428 is $AW(CaSO_4)$-AW(lime).

The assumptions of the calculation are that the total ash is the sum of the ash from the separate components, the calcium from the RDF does not bind sulfur as $CaSO_4$, and the lime that is not converted to $CaSO_4$ is rehydrated to $Ca(OH)_2$ in the final ash.

To take into account calcium loss, the calcium balance ratios are assumed to be correct and the calcium loss is assumed to be due to loss of the original lime by entrainment in the product gas stream and deposition in the flow lines and/or filters down stream of the collector. All $CaSO_4$ and calcium contributed by the RDF is arbitrarily assumed to remain in the ash. The mass of lime is corrected for loss by multiplying by the factor (Ca in ash - Ca in RDF)/(Ca in lime) using values given in table 4.

11.4 Effective Ash Temperature.

The partial pressure of SO_2, P_{SO2}, and O_2, P_{O2}, for the equilibrium constant K_{eq}, equation (1b) of the text, were calculated as:

$$P_{SO2} = N_{SO2}P_{com}/[N_{out}(dry)+N_W + N_{WV}]$$

$$P_{O2} = [N_{in}X_{O2}-N_{O2}(con)]P_{com}/[N_{out}(dry)+N_W + N_{WV}]$$

where N_{SO2}, $N_{out}(dry)$, N_{WV}, and N_{in} have been defined in appendix 11.2 and are calculated according to equations (11-1) through (11-11). N_W is the rate of production of water that remains trapped in the collector plus cold trap, X_{O2} is the mole fraction of O_2 in the inlet oxidant gas, $N_{O2}(con)$ is the molar rate of consumption of oxygen during the combustion, and P_{com} is the combustor pressure. The value of N_W is given by :

$$N_W = n_W(N_{CO2}+ N_{CO})/ma \qquad (11\text{-}13)$$

where n_W is the total moles of water trapped in the collector and cold trap, N_{CO2} is the molar rate of production of CO_2, N_{CO} is the molar rate of production of CO, and ma is the total moles of carbon dioxide plus carbon monoxide produced during the combustion (see equation (11-4)). In equation (11-13), it is assumed that the residual moisture, which is about 5% of the total water produced, is vaporized at a rate proportional to the combustion rate. The molar rate of consumption of oxygen is given by:

$$N_{O2}(con) = Z_1(N_{CO2}+N_{CO})-N_{CO}/2$$

where

$$Z_1 = 1+b/4a-c/2a+d'/a+3d''/2a-f/4a$$

and the parameters a, b, c, d', d", and f are as defined for the combustion reaction, equation (11-4), and are calculated as described in appendix 11.2. In our experiments n_W/ma is about 0.38 and Z_1 is about 1.16.

The error estimate for T_{eq} was calculated as follows. Assuming an uncertainty of 10% in X_{CO2}, 10% in P_{com}, and 5% in X_{O2}, the estimated error in K_{eq} is 27%. Using equation (2) of the text, this results in an error of $(1200)^2 x 0.27/57701$

= 7K in T_{eq}. This 7K was added to a) the uncertainty of representation of the thermodynamic data by equation (2) of the text of 10K plus b) another 10K due to uncertainty in the thermodynamic data itself. This gives an overall error estimate of 27K in T_{eq} which we have rounded to 30K.

In calculating T_{eq}, the value of N_{SO2} was adjusted so that the sulfur balance ratio for each experiment is one. This alters the ash temperature, T_{eq}, by 10K. The rate of sulfur capture in slpm, shown in figures 10 and 11, is calculated as the SO_2 if no lime were present minus the observed SO_2. The molar rate of SO_2 produced when no lime is present, n'_{SO2}, is calculated from:

$$n'_{SO2}=(n_{S,ash}+ n_{SO2})(N_{CO2}+ N_{CO})/ma$$

where $n_{S,ash}$ is the moles of sulfur captured by the lime and n_{SO2} is the moles of SO_2 gas.

11.5 Gas Thermocouples

11.5.1 Introduction

Some simple linear models were used to estimate the difference between the observed temperature and the true gas temperature and are discussed in detail because of the importance of the result. The gas thermocouple in its insulator without its surrounding aspiration tube, the usual arrangement, is referred to as the regular thermocouple. When the aspiration shield is in place, the thermocouple is referred to as the aspirated thermocouple. The model for the regular thermocouple is considered first and then the model for the aspirated thermocouple in combination with an analysis of the aspiration experiment carried out in experiment 112 is described.

11.5.2 Model for the Regular Gas Thermocouple

To estimate temperature corrections for the regular thermocouple, we assume the radial temperature gradients are negligible in comparison to axial temperature gradients within the thermocouple. The energy balance equation for the thermocouple at each position x is given by equation (11-14) of table 7. In equation (11-14), T_e is the radiant temperature of the environment, T is the temperature of the thermocouple, σ is Planck's constant, ϵ is the emissivity of the surface of the thermocouple, D is its diameter, h_g is the convective heat transfer coefficient per unit area, T_g is the gas temperature, and D_g is the diameter of the boundary layer around the thermocouple. The parameter k is the thermal conductivity and the parameter a is the cross sectional area. We assume D_g = D and that the values of T_g and T_e are constant and independent of position.

Radiant heat transfer is linearized as indicated by equations (11-15); T_a is an "average" temperature selected for evaluating the heat transfer coefficient. The heat transfer coefficient for gas convection, h_g, is evaluated using equations (11-16). The parameter $k_g(T_g)$ is the thermal conductivity of the gas at the absolute temperature T_g, Re is the corresponding Reynolds number, and D and b are constants. The parameter nv_0 is

the velocity of flow past the thermocouple tube expressed as some multiple n of the drift velocity v_0. The parameter δ is the kinematic viscosity of the gas.

Since the thermocouple junction and first 0.7 cm of its leads are bare, the temperature of the thermocouple is approximated as the solution of equation (11-14) for the case where ϵ, D, h_g, k, and a have values corresponding to the bare wire between x=0 and x=l'=0.7 cm and to a different set of values ϵ', D', h_g', k', and a' which represent the combination of the insulator and wire (which we call the ins/wire model) between x=l' and x=l=9.5 cm. The temperatures in the two regions are referred to as T(x) and T'(x). The boundary conditions are given in equations (11-17).

The reason for explicit inclusion of the fact that the first 0.7 cm of thermocouple is bare can be seen directly from the algebraic form of the solution to equations (11-14) and (11-17) at x=0, T(0), which is given by equation (11-22) in table 9. The parameters A_g and A are for the bare wire and A_g' and A' are for the ins/wire. The first two terms (terms are labeled by Roman numerals) on the right hand side (r.h.s.) of equation (11-22) determine whether or not the thermocouple junction behaves more closely as a bare wire or a bare wire encased in the insulator. This can be established by noting that when l' goes to zero, the first two terms reduce to $A_g'Z_g/A'$, the expression for the ins/wire model. When l' approaches l, $\cosh\theta'$ goes to 1 and Q gets large. Thus, the second term becomes much smaller than the first, A_gZ_g/A, and when added to the fourth term on the r.h.s. of equation (11-22) gives the expression for a completely bare wire of length l. The question at issue was whether the thermocouple behaved more like it was a bare wire or a wire completely covered by insulator.

The term involving Z(l) on the r.h.s. of equation (11-22) is the immersion error, Z(0) when Z_g is zero.

Parameters used to evaluate equations (11-14) and (11-17) are given in values of paramters and the equations (11-18) in the bottom half of table 7. For the bare wire, we calculated h_g using the diameter of a single wire and doubled the value for both the radiant and convective heat transfer to account for both wires. The area, a, is for two wires. The thermal conductivity , k,wire, is for platinum. The product ka of the combined wire/insulator portion is the sum of the separate products for each of the wires and the insulator. The thermal conductivity of the alumina insulator, k,ins, is a linear interpolation between the values at 800 °C and 24 °C supplied by the manufacturer. The thermal conductivity of the insulator wire combination, k,eff, is the sum of that for the wire and the insulator weighted according to their respective areas. The value of f was evaluated at 300 °C to be consistent with the model of the aspirated thermocouple and not because the temperature of the wire is close to this value. We assumed that flow of the product gas is perpendicular to the thermocouple or insulator and used values for a and b from King's studies[b] for Re<100. The drift velocity v_0 was

[b] See Jakob, Max, "Heat Transfer", p561. Vol I, John Wiley and Sons, Inc., London, 1949

calculated using the inner diameter of the combustor of 41 cm and assuming the product gas is leaving the combustor at a rate of 210 slpm. Calculations were made for n=1 and n=5. The value of T(0) was kept constant at 600 °C (873K) for reasons that will be evident below, and equation (11-14) was solved for various values of $X=T_e-T(0)$ to obtain corresponding values of $Y=T(0)-T_g$. The results can be expressed in the form of equation (11-23).

$$Y = (c_1 + c_2X)(X+Y) + (b_1 + b_2X) \qquad (11\text{-}23)$$

The results for the range $-200 \leq X \leq 200$ are given under the heading of model II in table 10.

The corresponding values for the parameters for a bare wire having a length of 9.5 cm are given under the heading of model VI and for the ins/wire model with the junction covered with insulator under model V of table 10. Thus, the regular thermocouple characteristics, model II, are intermediate between the bare wire, model VI, and the covered wire, model V. The negative of b_1+b_2X is the immersion error.

It is clear that the formula used for summarizing the calculations in table 10, equation (11-23), results in a single equation with two unknowns, T_e and T_g, since T(0) is the temperature registered by the thermocouple junction. To obtain a second equation to solve for the unknowns, we looked at the results of the aspiration experiment.

11.5.3 The Aspiration Experiment

The results of the aspiration experiment during run 112 are shown in figure 12. The temperatures of the aspirated and the regular gas lower side thermocouples are plotted as a function of time in curves A and B, respectively. The thermocouple in the aspiration shield is called the aspirated thermocouple whether the aspiration flow rate is zero or not. In the lower half of the figure the temperature of the aspirated minus the regular thermocouple and the aspiration flow rate are plotted as a function of time in the difference curves C and D, respectively. This temperature difference is used to at least semi-quantitatively cancel out variations in temperature due to variations in heat release.

According to the difference plot, curve C, the regular and aspirated thermocouple temperatures, apart from expected lags, are within 10-20 °C, when the aspiration flow rate is zero. This result was unexpected since it suggests that the gas and radiant temperature are nearly equal, and thus, fortuitously, the difference between the observed (i.e., with a regular thermocouple) and actual gas temperature ought to be small. In any event, the additional measurement with the aspirated thermocouple should be sufficient to provide a second relation of the form of equation (11-23).

The main plateau of values for the regular side gas thermocouples is near 600 °C; hence, the reason for the selection of 600 °C for T(0) in the preceding calculation.

11.5.4 Model for the Aspiration Thermocouple (No Aspiration)

The aspiration thermocouple is mounted inside an aspiration tube. The model adopted for the case when no gas is aspirated is that the thermocouple can be approximated by the combination of insulation/wire described above over its full length. This keeps the algebra reasonably simple and is justified on the basis that details of the heat transfer to the thermocouple junction are relatively unimportant; the junction will, apart form an immersion error, register the temperature of the end of the aspiration tube.

The energy balance equations, neglecting radial temperature gradients within the aspiration tube and thermocouple, are given by equations (11-19) of table 8. In these equations, T_1 is the temperature of the aspiration tube and T_2 is the temperature of the thermocouple, and similarly for the subscripted symbols k, a, and D. D_1' is the diameter of the hole in the aspiration tube, and D_2 is the diameter of the ins/wire model of the regular thermocouple. The parameter H_{12} is a heat transfer coefficient per unit axial length and was estimated to be the sum of that by conduction and radiation between the thermocouple and shield as given by equations (11-20). Equations (11-20) neglect heat transfer between locations on the shield and thermocouple that are not at the same value of x; the error is such that the heat transfer is overestimated towards x=0 and underestimated towards x=1.

Solving equations (11-19) with the boundary conditions (11-21) gives the results listed for model I of table 10. The numerical value of c_1 indicates the aspiration couple registers a temperature nearer T_e than T_g than the regular thermocouple. (Neglecting c_2X and b_2X in comparison to c_1 and b_1, respectively, equation (11-23) becomes $T(0) = c_1T_e + (1-c_1)T_g + b_1$.)

Calling T(0) for the aspirated couple and regular thermocouple T_a and T_r, respectively, models I and II were used to determine T_e-T_r and T_e-T_g for various values of T_r-T_a. The results for the two flow velocities are given at the bottom of table 10. The average value of T_r-T_a for the time from 57 to 79 minutes in the aspiration experiment, which just precedes the first actual aspiration of gas through the thermocouple, is +12 °C. This suggests that T_r-T_g and T_e-T_g are between 0 and -1 °C and -5 and -6 °C, respectively. During the time interval preceding the last aspiration from 115 to 124 minutes, T_r-T_a is +24 °C which places T_r-T_g from -24 to -9 °C and T_e-T_g between -2 and -36 °C.

Curve C of figure 12 shows that there is an increase of ~55 °C in the first and ~30 °C in the second aspiration but essentially none in the third aspiration. Moreover in the first two aspirations, the change in temperature with flow rate above 17 slpm is insignificant. Our interpretation is as follows. For the aspiration flow rates we used, the aspirated couple registers the temperature of the aspirated gas with an estimated error less than 5 °C. Because the aspiration flow rate greatly exceeds the probable isokinetic sampling rate, the local flow pattern of gas is altered from that present at zero aspiration flow rate. More inlet oxidant gas relative to the hotter product gas is being pulled into the aspiration tube as the aspiration flow rate increases. In the third aspiration, we see no temperature rise because at the start of the third aspiration, the CO_2 production is dropping rapidly. We

have already inferred from the lower pellet thermocouple data that the ash and burning sample are falling into the ash pan. Thus, the hot product and inlet oxidant gas are already relatively well mixed and no temperature rise occurs.

11.5.5 Discussion

To determine the effect of neglecting the temperature difference between the wire and the insulator in the ins/wire model, equations (11-19) were used to evaluate the performance of a wire completely covered with insulator. The results are listed as model IV in table 10. Comparison with the results of model V, where this difference is neglected, shows the error is small. The use of a value of T_a for the bare junction that is close to its actual temperature, 600 °C, results in a small change in the parameter c_1 as indicated by model II versus model III of table 10.

The linearization of radiant heat transfer using a T_a of 300 °C in combination with the neglect of the variation of k,eff with temperature of the models means that the effective radiative heat transfer is underestimated by a factor of 2.47 at 600 °C and overestimated by a factor of 2.2 at room temperature. The term for convective heat transfer is underestimated by a factor of 1.47 at 600 °C and overestimated by a factor of 1.3 at room temperature due to the temperature variation of k,eff of the model. Thus, the models underestimate the radiative relative to the convective heat transfer term; the shift in results would be towards larger values of the parameter c_1+c_2X. Since c_1+c_2X is bounded (i.e., it must be less than one), it follows that values of T_e-T_g will be, in reality, larger for a given value of T_r-T_a than our estimates. A change by a factor of two in the values of T_e-T_g might be expected for a given value of T_r-T_a. Thus, we estimate the magnitude of T_e-T_g to be within 100 °C after aspiration and prior to burnout and T_r-T_g to be within 50 °C.

12. Acknowledgements

The authors wish to thank the U.S. Department of Energy Office of Renewable Energies Technology, Energy from Municipal Solid Waste division for funding during FY 1989-1990. The authors wish to thank Mr. Oscar O. Ohlsson of ANL and Dr. Kenneth Daugherty of NTSU for samples of the coal and RDF used in the ANL/NTSU incinerator tests. The authors also wish to thank Dr. Gerald Mitchell and Mr. William Dorko of NIST for their assistance in both checking the concentrations of the SO_2 calibration gases and the loan of a tank of one of these gases. The authors wish to thank Mr. George Burns for consultation on making temperature measurements with thermocouples and Ms. Margaret Skroger of NIST for instruction on welding thermocouple junctions. We wish to thank Mr. Thomas L. Jobe, Jr. of NIST for assistance in searching the NSRDS files for thermal functions pertinent to this work. We are indebted to Dr. Eugene S. Domalski of NIST for guidance and discussions, and Dr. Allen E. Van Til of UOP Research Center who discussed the SO_2 capture problem and provided us with the results of his analysis of the problem. The authors wish to thank Mr. Albert E. Ledford, Jr.,of NIST, normally a collaborator but now assigned to other duties, who provided guidance in repair of the combustor which he originally engineered and assembled. Finally, the authors wish to thank Dr. Stanley Abramowitz of NIST for his support of our effort to complete this study.

Table 1 Pellet Composition, Properties of Coal and RDF

Experiment	Note	109	110	111	112	96	96	97	97	98
Pellet										
Total Mass, kg		2.248	2.064	1.999	1.985					
Coal, mass % ar	1	51.10	51.02	53.01	53.11					
RDF, mass % ar		41.84	41.72	43.30	43.39					
Lime, mass % ar		7.06	7.06	3.50	3.50					
MnO2, mass % ar		0.00	0.20	0.20	0.00					
Analyst	2	G	G	G	G	G	S	G	S	G
Coal										
Moist., mass % ar	3	4.60	4.51	4.63	4.13	5.13	6.62	4.84	6.89	5.26
Ash, mass % ar	4	(7.0)	(7.0)	(7.0)	7.22	6.12	5.89	6.38	6.36	6.58
Tot.Cl, mass % ar		0.03	0.02	0.04	0.04	0.01	0.01	0.01	0.01	0.01
Cl- , mass % ar	5	0.03	0.02	0.04	0.03	0.01	0.00	0.01	0.00	0.01
Tot. S, mass % ar		2.85	3.12	2.62	3.00	3.02	2.82	2.91	2.70	2.96
RDF										
Moist., mass % ar	3	4.70	2.86	2.24	4.60	---	---	4.79	---	---
Ash, mass % ar		9.80	9.71	9.30	9.05			9.08		
Tot.Cl, mass % ar		0.36	0.41	0.43	0.33			0.39		
Cl-, mass % ar	5	0.16	0.17	0.13	0.11			0.13		
Tot. S, mass % ar		0.24	0.35	0.32	0.32			0.23		
Tot. Ca,mass % ar		0.74	0.66	0.67	0.61			0.63		

1 ar; as received
2 G: Gascoyne Laboratory, S: Spots, Stevens, and McCoy
3 Residual moisture
4 () assumed ash content
5 Water soluble chlorine

Table 2 Chlorine Balance

Experiment	-------109-------			-------110-------			-------111-------			-------112-------			All
Lime, % ar	7.06			7.06			3.50			3.50			
MnO2, % ar	0.00			0.20			0.20			0.00			
	Amount		Uncert.	Amount		Uncert.	Amount		Uncert.	Amount		Uncert.	Uncert.
	ppm	g	g	ppm	g	g	ppm	g	g	ppm	g	g	ppm
Chlorine In:													
1 Tot. Cl coal	300	0.34	0.23	200	0.21	0.21	400	0.42	0.21	400	0.42	0.21	200
2 Tot. Cl RDF	3600	3.39	0.19	4050	3.49	0.17	4300	3.72	0.17	3300	2.84	0.17	200
3 Tot. Cl lime	150	0.02	0.02	150	0.02	0.02	150	0.01	0.01	150	0.01	0.01	150
4 Cl- coal	300	0.34	0.11	200	0.21	0.11	400	0.42	0.10	300	0.32	0.11	100
5 Cl- RDF	1600	1.50	0.09	1650	1.42	0.09	1300	1.13	0.09	1100	0.95	0.09	100
6 Cl- lime	150	0.02	0.02	150	0.02	0.02	150	0.01	0.01	150	0.01	0.01	150
7 Tot. Cl In		3.75	0.44		3.72	0.41		4.15	0.40		3.27	0.39	
Chlorine Out:													
8 Tot. Cl ash	400	0.13	0.06	400	0.12	0.06	0	0.00	0.04	200	0.04	0.04	200
9 Cl- ash	400	0.13	0.04	400	0.12	0.04	0	0.00	0.02	100	0.02	0.02	100
10 Tot. Cl cond.		3.18	0.15		3.49	0.23		3.96	0.21		3.68	0.18	
11 Tot. Cl Out		3.31	0.21		3.61	0.29		3.96	0.26		3.72	0.22	
	Value		Uncert.	Value		Uncert.	Value		Uncert.	Value		Uncert.	
12 (Tot. Cl In)/ (Tot. Cl Out)	1.13		0.20	1.03		0.20	1.05		0.17	0.88		0.16	
13 (Tot. Cl ash)/ (Tot. Cl Out)	0.04		0.02	0.03		0.02	0.00		0.02	0.01		0.02	
14 (Cl- ash)/ (Tot. Cl ash)	1.00		0.25	1.00		0.25	---			0.50		0.50	

Table 3 Sulfur Balance

	Experiment	109			110			111			112			All
	Lime, % ar		7.06			7.06			3.50			3.50		
	MnO2, % ar		0.00			0.20			0.20			0.00		
		Amount		Uncert.	Amount		Uncert.	Amount		Uncert.	Amount		Uncert.	Uncert.
	Sulfur In:	%	g	g	%	g	g	%	g	g	%	g	g	%
1	Tot. S coal	2.85	32.7	1.2	3.12	32.9	1.1	2.62	27.8	1.1	3.00	31.6	1.1	0.10
2	Tot. S RDF	0.24	2.3	0.1	0.35	3.0	0.1	0.32	2.7	0.1	0.32	2.7	0.1	0.01
3	Tot. S lime	0.01	0.0	0.0	0.01	0.0	0.0	0.01	0.0	0.0	0.01	0.0	0.0	0.01
4	Tot. S In		35.0	1.3		35.9	1.2		30.5	1.2		34.3	1.2	
	Sulfur Out:													
5	Tot. S ash	4.62	15.1	0.7	5.10	15.3	0.6	3.34	7.4	0.4	2.75	5.7	0.4	0.2
6	ash,corr.	do	15.1		do	13.7		do	7.1		do	5.3		
7	Tot. S cond.		2.9	0.1		5.4	0.2		2.5	0.2		6.5	0.2	
8	Tot. S SO2, meas.		---	---		18.5	4.2		29.9	6.9		27.5	6.3	
9	Tot. S SO2, calc.		17.0	2.0		15.2	2.0		20.6	1.8		22.1	1.7	
10	Tot. S Out		---	---		39.2	5.1		39.7	7.5		39.7	6.9	
		Value			Value			Value			Value			
11	(Tot. S In)/ (Tot. S Out)		(1.00)	--- / ---		0.92	0.15		0.77	0.17		0.86	0.18	
12	(Tot. S ash)/ (Tot. S Out)		(0.43)	0.08		0.39	0.05		0.18	0.04		0.14	0.03	
13	(Tot. S ash)/ (Tot. S In)		0.43	0.08		0.43	0.07		0.24	0.10		0.17	0.11	
14	(Tot. S SO2, meas.)/ (Tot. S Out)		(0.49)	0.16		0.47	0.07		0.75	0.06		0.69	0.06	
15	(Tot. S cond.)/ (Tot. S Out)		(0.08)	0.08		0.14	0.03		0.06	0.02		0.16	0.04	
16	(moles S in ash)/ (moles lime)		0.219	0.009		0.243	0.010		0.243	0.015		0.188	0.014	
17	(Tot. S SO2, calc.)/ (Tot. S SO2, meas.)		---	---		0.82	0.36		0.69	0.32		0.80	0.31	

Table 4 Calcium Balance

Experiment	-------109-------			-------110-------			-------111-------			-------112-------			All
	%	Amount g	Uncert. g	%	Amount g	Uncert. g	%	Amount g	Uncert. g	%	Amount g	Uncert. g	Uncert. %
Calcium In:													
1 Tot. Ca coal	---	---	---	---	---	---	---	---	---	---	---	---	
2 Tot. Ca RDF	0.735	6.91	0.09	0.655	5.64	0.09	0.665	5.76	0.09	0.605	5.21	0.09	0.01
3 Tot. Ca lime	53.6	85.05	0.32	53.6	78.08	0.29	53.6	37.46	0.14	53.6	37.25	0.14	0.20
4 Tot. Ca In		91.96	0.41		83.72	0.38		43.21	0.54		42.46	0.23	
Calcium Out:													
5 Tot. Ca ash	22.0	71.68	6.52	23.5	70.45	6.00	18.4	40.50	4.40	17.0	35.07	4.13	
6 Tot. Ca cond.		0.00	0.04		0.03	0.07		0.02	0.06		0.14	0.05	
7 Tot. Ca Out		71.68	6.56		70.48	6.07		40.52	4.46		35.21	4.18	
		Value			Value			Value			Value		
8 (Tot. Ca In)/ (Tot. Ca Out)		1.28	0.12		1.19	0.11		1.07	0.13		1.21	0.15	

Table 5 Calculated versus Observed Ash

	Experiment	-------109-------			-------110-------			-------111-------			-------112-------			All
			Amount	Uncert.		Amount	Uncert.		Amount	Uncert.		Amount	Uncert.	Uncert.
		%	g	g	%	g	g	%	g	g	%	g	g	%
	Ash Calculated:													
1	coal*	(7.0)	80.4	2.3	(7.0)	73.7	2.1	(7.0)	74.2	2.1	7.22	76.1	2.1	0.2
2	RDF	9.8	92.2	0.1	9.71	83.6	0.9	9.3	80.5	0.9	9.05	77.9	0.9	0.1
3	MnO2		0			4.2	0.4		4.0	0.4		0		10
4	lime	100	158.6	0.2	100	145.6	0.1	100	69.9	0.01	100	69.6	0.1	0.1
5	CaSO4		32.5	0.8		33.6	0.7		15.8	0.5		12.6	0.5	
6	CaSO4, <Ca **		28.8	0.7		30.9	0.7		15.4	0.5		11.8	0.5	
7	Total, CaSO4		363.7	4.0		340.7	4.3		244.4	3.9		236.1	3.5	
8	Total, CaSO4,<Ca		322.1	4.0		313.3	4.3		239.0	3.9		223.3	3.5	
9	Ash Observed:		325.8			299.8			220.1			206.3		

* () is assumed ash content

**<Ca: calcium loss from ash, assumes Ca lost from ash is only Ca from lime

Table 6 Average Temperatures of Wall and Gas in Combustion Zone

Experiment	109		110		111		112	
	Wall	Gas	Wall	Gas	Wall	Gas	Wall	Gas
Gas in port		430		400		379		410
Baffle	369		341		343		352	
Upper wall	284		258		266		267	
Middle wall	475		431		432		439	
Gas upper side		532		488		473		492
Lower wall	493		448		478		460	
Gas lower side		548		496		494		476
Gas lower side		540		490		488		---
Ash Pan*	454		408		---		---	
Pyrometer								
Avg when on	1020		974		1000		1007	
% time on	80		82		43		60	
Init. peak	1258		1470		1371		1370	
Main Peak	1247		1188		1475		1110	

*Ash Pan thermocouple opened in expts 111,112.

Table 7 Model of Regular Thermocouple

Energy Balance: $(T_e^4 - T^4)\sigma\epsilon\pi D + h_g(T_g - T)\pi D_g + (ka)d^2T/dx^2 = 0$ (10-14)

Radiation: $T_e^4 - T^4 = 4T_e^3 f(T_a)(T_e - T)$ (10-15a)

$f(T_a) = 1 - 1.5Z_a + (Z_a)^2 - 0.25(Z_a)^3$ (10-15b)

$Z_a = (T_e - T_a)/T_e$ (10-15c)

Gas convection: $h_g = k_g(T_g)bRe^d/D$ (10-16a)

$Re = nv_0 D/\delta$ (10-16b)

Conditions: $x=0 \quad dT/dx=0$ (10-17a)

(Bare wire) $0 \le x \le l'$ $T(x)$; T_e, T_g, ϵ, D, f, h_g, k, a independent of x

$x=l' \quad T(l') = T'(l'); \quad kadT/dx = k'a'dT'/dx$ (10-17b)

(Ins/wire) $l' \le x \le l$ $T'(x)$; T_e, T_g, ϵ', D', f', h_g', k', a' independent of x

(Combustor wall) $x=l \quad T' = 0\ ^\circ C$ (10-17c)

Values of parameters: $T(0) = 600\ ^\circ C$, $l' = 0.7$ cm, $l = 9.5$ cm

ϵ	.2	ϵ'	.8
D	.0254 cm	D'	.159 cm
f	$T_a = 300\ ^\circ C$	f	$T_a' = 300\ ^\circ C$
k	k,wire(600 °C)	k'	k,eff(300°C)
a	1.01×10^{-3} cm^2	a'	18.33×10^{-3} cm^2

$k,wire = .695(1 + 2.84 \times 10^{-4} T)$, T in °C, W/cm/K (10-18a)

$k,ins = .332(1 - 9.55 \times 10^{-4}(T - 24))$, T in °C, W/cm/K (10-18b)

$k,eff = (1.01 \times k,wire + 17.32 \times k,ins)/18.33$, T in °C, W/cm/K (10-18c)

$n=1$, $v_0 = 2.70(T_g \text{ in K}/273)$ cm/sec, $b = .764$, $d = .41$ (10-18d)

$\delta = .13(T_g/273)^{1.5}(1 + 139/273)/(1 + 139/T_g)$, T_g in K, cm^2/sec (10-18e)

$k_g(T_g) = 24.9(T_g/273)^{.5}[(1 + GT_g)/(1 + 273G)][(1 + C/273)/(1 + C/T_g)]$ (10-18f)

$G = 8.9 \times 10^{-5}$, $C = 139$, T_g in K, W/cm/K.

Table 8 Model of Aspiration Thermocouple
(No Aspiration Flow)

Energy Balance:

Tube: $H_{12}(T_2-T_1)+(T_e^4-T_1^4)\sigma F_e \pi D_1 + h_g(T_g-T_1)\pi D_g + k_1 a_1 d^2T_1/dx^2 = 0;\ 0\le x\le 1$ (10-19a)

Thermocouple: $H_{12}(T_2-T_1) + k_2 a_2 d^2T_2/dx^2 = 0;\ 0\le x\le 1$ (10-19b)

H_{12}: $T_2^4-T_1^4 = 4T_e^3[f(Z_1)(T_e-T_1)-f(Z_2)(T_e-T_2)] = 4T_e^3 f(Z_a)(T_2-T_1)$ (10-20a)

$Z_a=(T_e-T_a)/T_e$ (10-20b)

$H_{12}=2\pi k_g(T_a)/\ln(D_1'/D_2) + \sigma 4T_e^3 f(T_a)\pi D_2/[1/\epsilon_2 + (1/\epsilon_1-1)D_2/D_1']$ (10-20c)

Conditions: $x=0$ $dT_1/dx=0$, $dT_2/dx=0$ (10-21a)

$0\le x\le 1$ T_e, T_g, ϵ_1, D_1, f, h_g, k_1, a_1,

ϵ_2, D_2, k_2, a_2 independent of x

$x=1$ $T_1 = 0$ °C, $T_2 = 0$ °C (10-21b)

Values of parameters: $T(0) = 600$ °C, $T_a = 300$ °C, $l = 9.5$ cm

ϵ_1	.8	ϵ_2	.8
D_1	.953 cm	D_2	.159 cm
f	T_a=300 °C	f	T_a=300 °C
k_1	k,ins(300 °C)	k_2	k,eff(300°C)
a_1	.396 cm^2	a_2	18.32×10^{-3} cm^2
D_1'	.635 cm		

See equations (10-18)

Table 9 Algebraic Formulae for Solutions to
Regular Thermocouple Models

$$Z(0) = A_g Z_g/A + \Gamma[\beta Z_g \cosh\theta'/Q + (Z(1)-Z_g A_g'/A')/Q] \qquad (10\text{-}22)$$

terms: I II III IV

$Z(x)=(T_e-T(x))/T_e$; $Z_g=(T_e-T_g)/T_e$

$A_g = h_g \pi D/ka$; $A = (h_r f_a+h_g)\pi D/ka$; $h_r=\epsilon\sigma 4T_e^3$;

$A_g' = h_g \pi D'/(k'a')$; $A' = (h_r' f_a+h_g')\pi D'/(k'a')$; $h_r'=\epsilon'\sigma 4T_e^3$;

$\Gamma=[(k'a)'/(ka)](A'/A)^{.5}$; $\beta = A_g'/A' - A_g/A$;

$Q= \sinh\theta\sinh\theta'+\Gamma\cosh\theta\cosh\theta'$; $\theta=1(A)^{.5}$; $\theta'=(1-1')(A')^{.5}$.

Table 10 Estimates of Radiation Corrections
for Gas Thermocouples

Summary of Model Calculations

Velocity	n=1	n=5	Notes
Model I: Asp. Thermocouple (Coupled, Junction covered)			2
c1	0.862	0.757	3
c2x100	0.067	0.075	
b1	-13.8	-10.3	
b2	0.070	0.049	
Model II: Reg. Thermocouple (Ins/wire, Junction Bare)			
c1	0.429	0.246	
c2x100	0.051	0.036	
b1	-0.100	-0.019	
b2x100	0.055	0.010	
Model III: Reg. Thermocouple (Ins/wire, Junction Bare) (Ta=600)			
c1	0.463		
c2x100	0.053		
b1	0.097		
b2x100	-0.053		

Velocity	n=1	n=5
Model IV: Coupled Ins/wire (Junction covered)		
c1	0.698	0.533
c2x100	0.080	0.071
b1	-0.073	-0.018
b2x100	0.044	0.010
Model V: Ins/wire (Junction covered)		
c1	0.681	0.526
c2x100	0.058	0.061
b1	-0.101	-0.025
b2x100	0.059	0.013
Model VI: Bare Wire		
c1	0.162	0.090
c2x100	0.037	0.020
b1	0.000	0.000
b2x100		

Estimate of Radiation Correction
(Models I and II)

	n=1		n=5	
Tr-Ta	Te-Tr	Te-Tg	Te-Tr	Te-Tg
30	-40	-69	-38	-50
20	-19	-32	-19	-26
10	4	7	-1	-1
0	27	48	18	24
-10	51	93	37	50
-20	76	140	56	76

Notes: 1) n is multiple of drift velocity; equation (10-18c).
2) Coupled refers to calculations based on equations (10-19).
3) Parameters are for equation:
$T(0)-Tg = (c1+c2*X)(Te-Tg) + (b1+b2*X)$
where $X = Te-T(0)$.
4) Tr is temperature indicated by the regular thermocouple.
5) Ta is temperature indicated by the aspirated thermocouple.

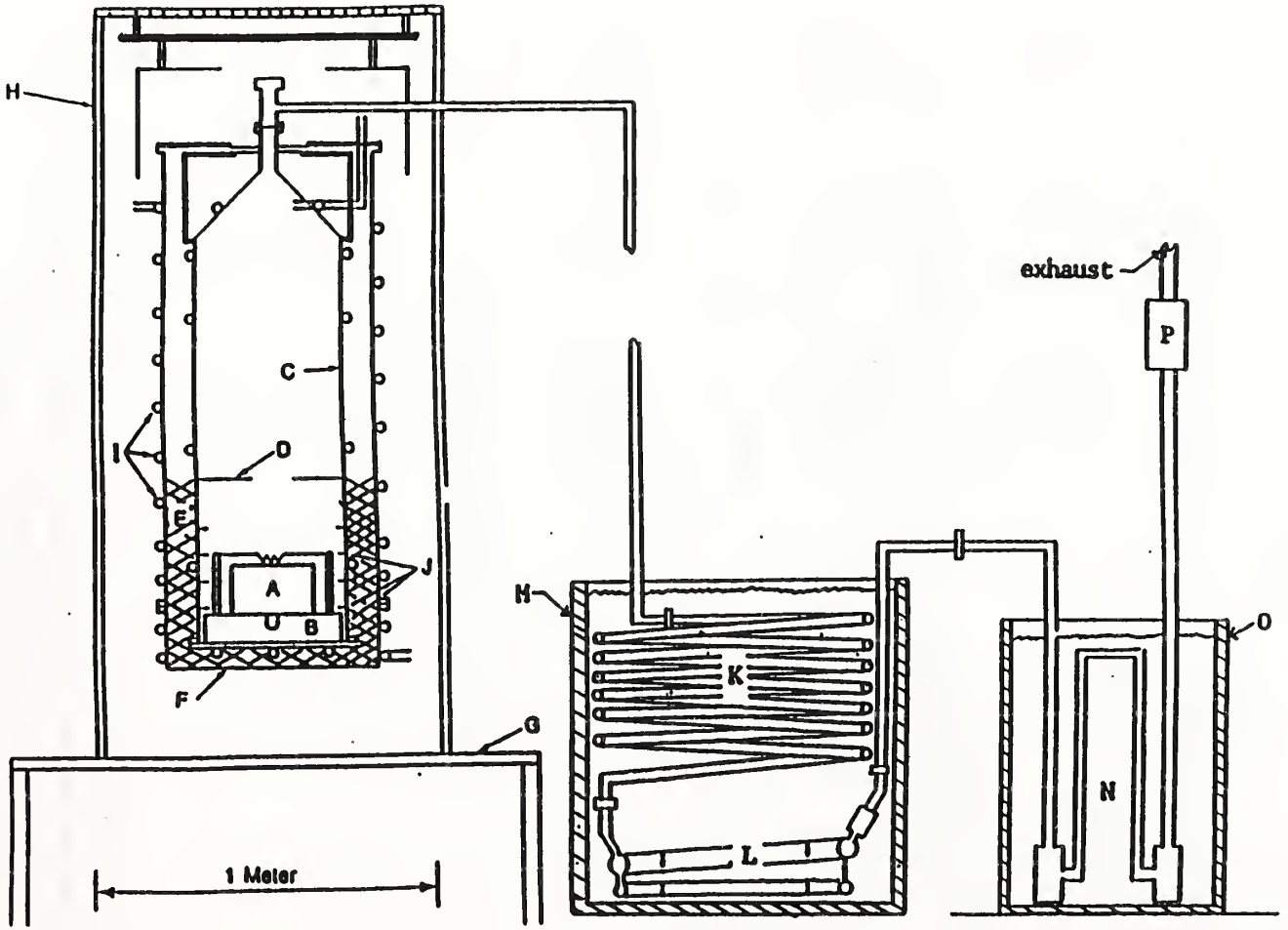

Figure 1 NIST COMBUSTOR
A, Sample pellet; B Ash pan with sample grate; C, Combustor; D, Baffle; E, Insulation; F, Combustor enclosure; G, Deck; H, Support frame; I, Cooling-water coils; J, Oxidant gas nozzles; K, Ten-turn heat exchange coil; L, Water collector; M, Water bath; N, Cold trap, O, Cold bath; and P, Charcoal trap.

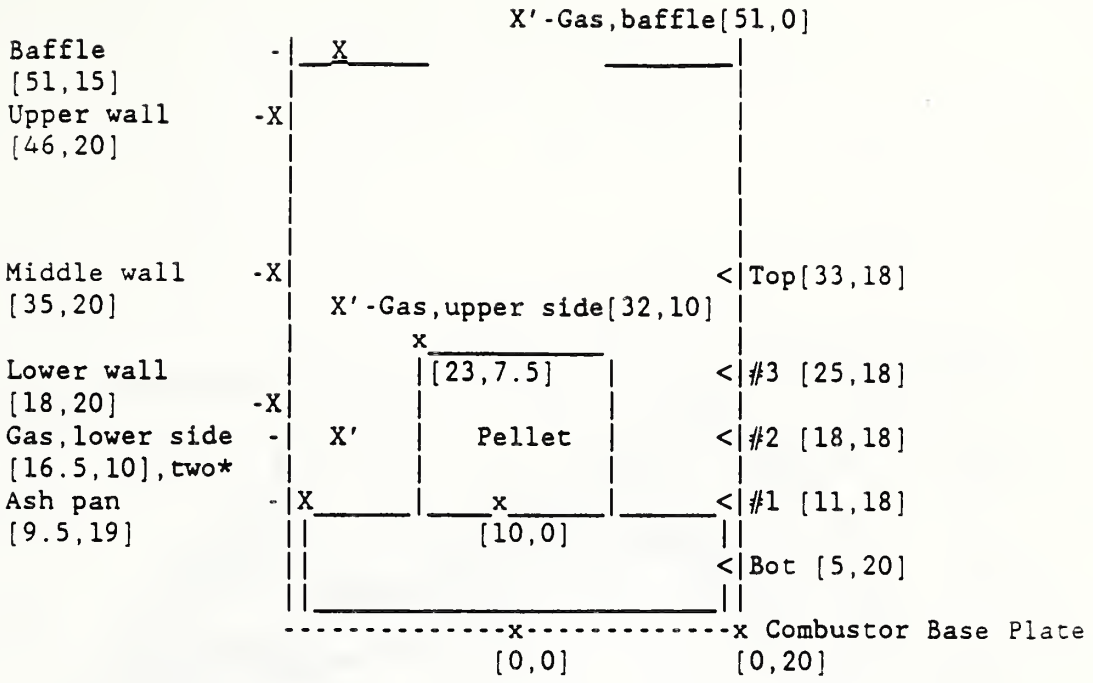

Fig. 2 Sketch of Thermocouple and Oxidant Gas Nozzle Locations
in
Combustion Zone (lower 1/3 of Combustor)

Notes:

X' indicates gas thermocouple junction location; noble metal thermocouples are located at gas,lower side, (two) and gas, upper side.

X indicates wall or other solid metal component thermocouple junction location.

< indicates location of outlet of ports of oxidant gas nozzle tier.

x indicates a position (i.e., top edge and bottom center of pellet, bottom center and bottom edge of base plate).

[a,b] indicates position by height,a, above combustor base plate and radial distance, b, from center of combustor base plate. All heights and radial distances are in cm.

* The two junctions are 60 degrees from each other.

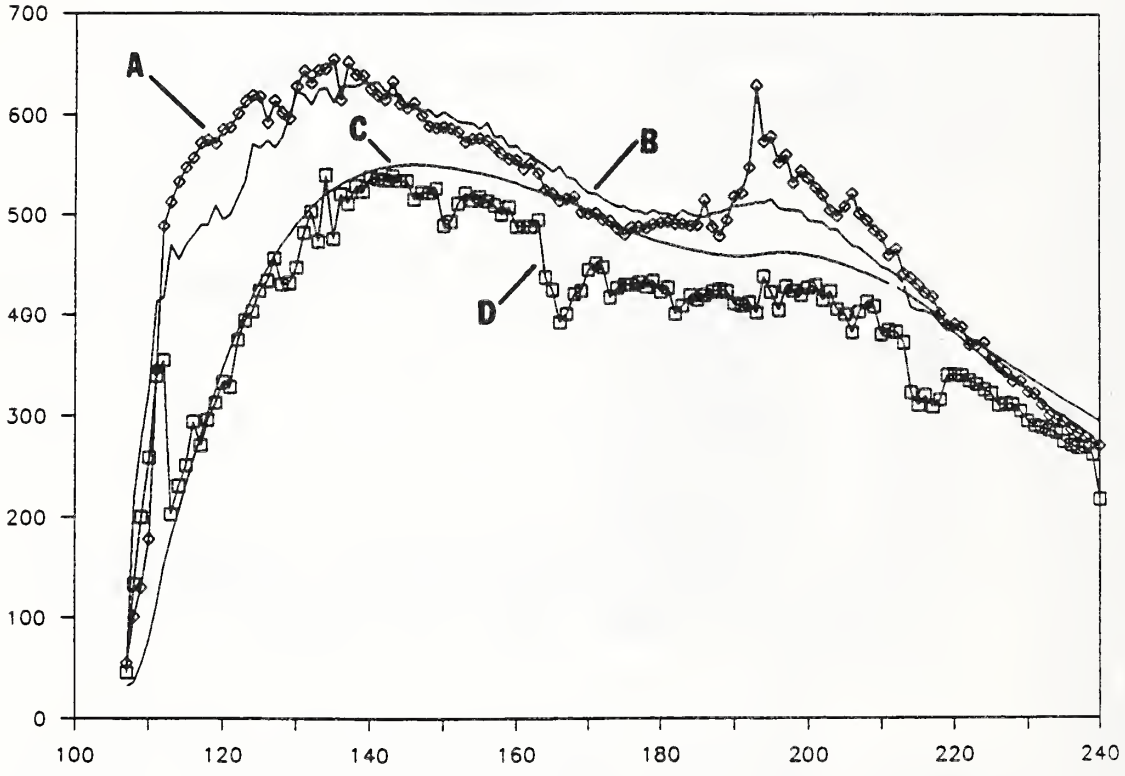

Figure 3 Gas and Middle Wall Temperatures versus Time
Experiment 110 (7.1% lime, 0.2% MnO_2)
Y axis: Temperature, °C; X axis: Arbitrary Time, minutes
A, Gas lower side thermocouple; B, Gas upper side thermocouple;
C, Middle wall thermocouple; and D, Gas baffle thermocouple.

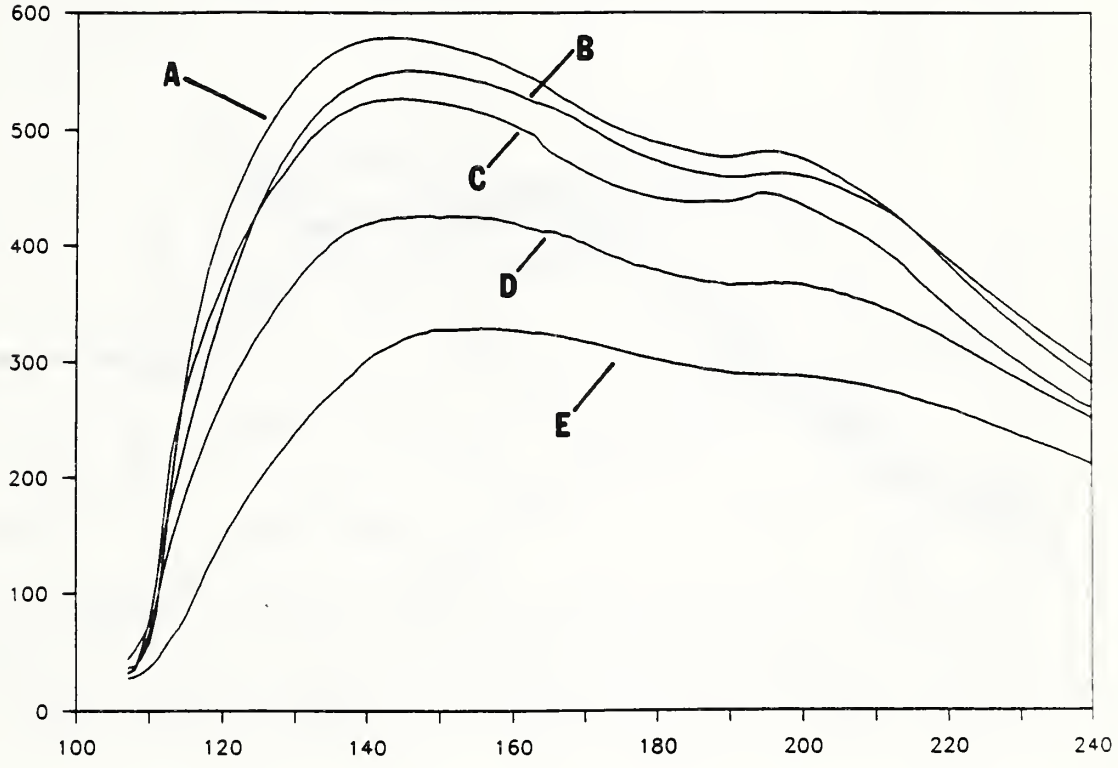

Figure 4 Combustor Wall, Ash Pan, and Baffle Temperature versus Time
Experiment 110 (7.1% lime, 0.2% MnO_2)
Y axis: Temperature, °C; X axis: Arbitrary Time, minutes
A, Lower wall thermocouple; B, Middle wall thermocouple; C, Ash Pan thermocouple; D, Baffle thermocouple; and E, Upper wall thermocouple.

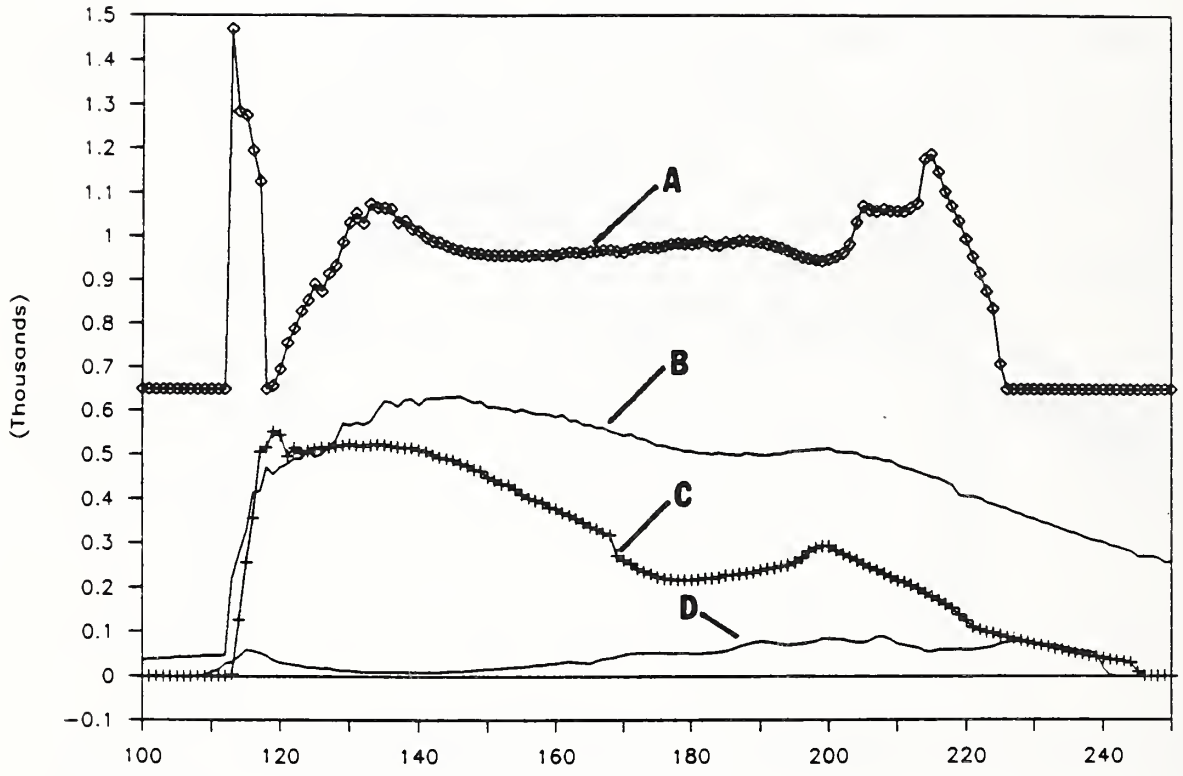

Figure 5 Sample Surface and Gas Upper Side Temperatures, CO_2 and CO Production Rates versus Time
Experiment 110 (7.1% lime, 0.2% MnO_2)
Y axis: arbitrary units, thousands; X axis: Arbitrary Time, minutes
A, Pyrometer temperature, °C; B, Gas upper side thermocouple °C;
C, CO_2 production rate, slpm x 20;
and D, CO production rate, slpm x 100.

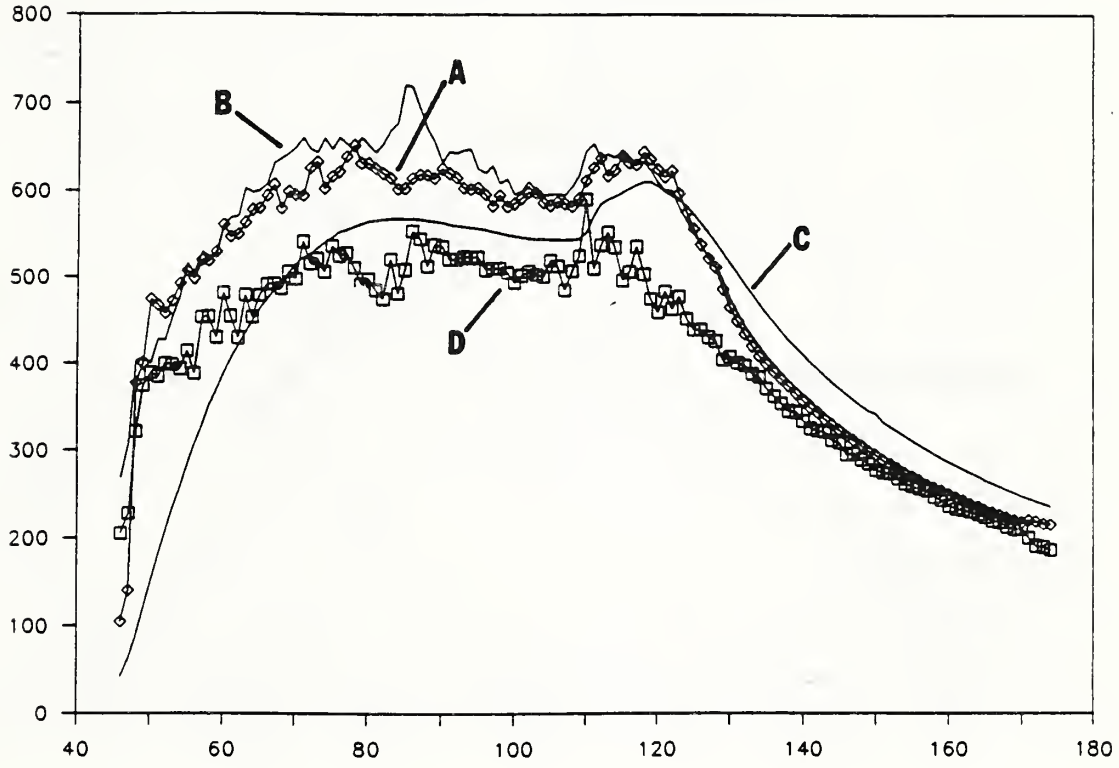

Figure 6 Gas and Middle Wall Temperatures versus Time
Experiment 112 (3.5% lime, 0.0% MnO_2)
Y axis: Temperature, °C; X axis: Arbitrary Time, minutes
A, Gas lower side thermocouple; B Gas upper side thermocouple;
C, Middle wall thermocouple; and D, Gas baffle thermocouple.

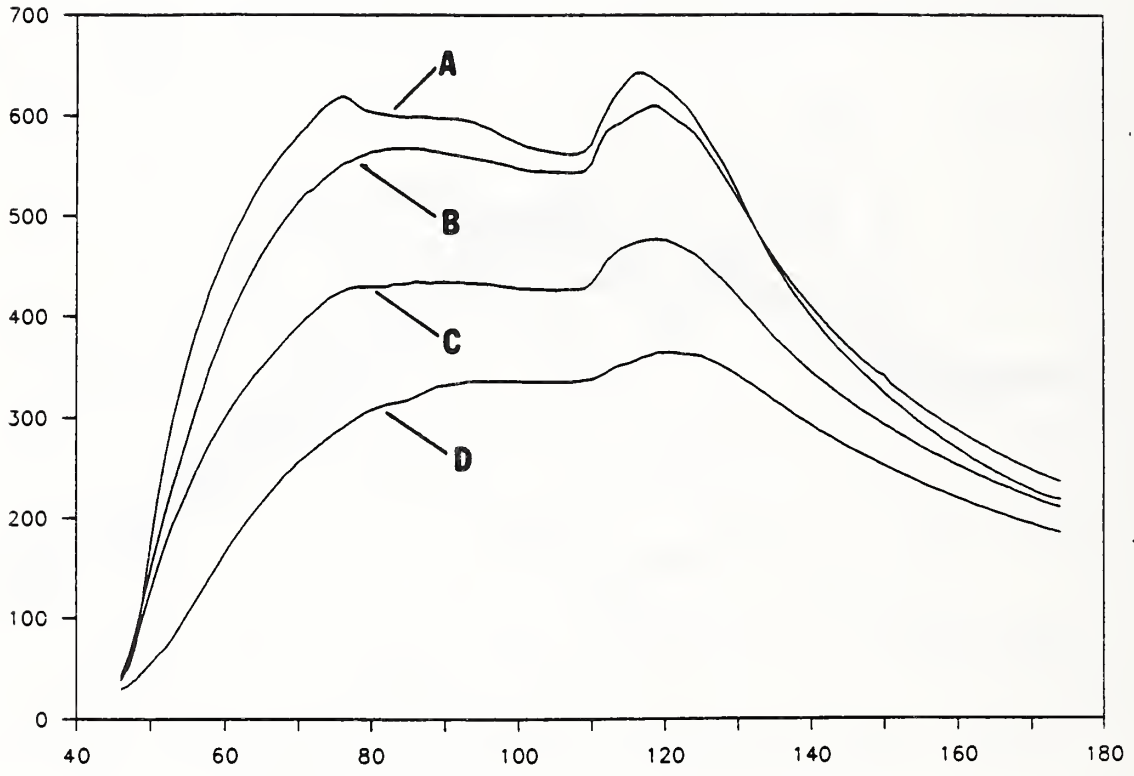

Figure 7 Combustor Wall and Baffle Temperatures versus Time
Experiment 112 (3.5% lime, 0.0% MnO_2)
Y axis: Temperature, °C; X axis: Arbitrary Time, minutes
A, Lower wall thermocouple; B, Middle wall thermocouple; C, Baffle thermocouple; and D, Upper wall thermocouple.

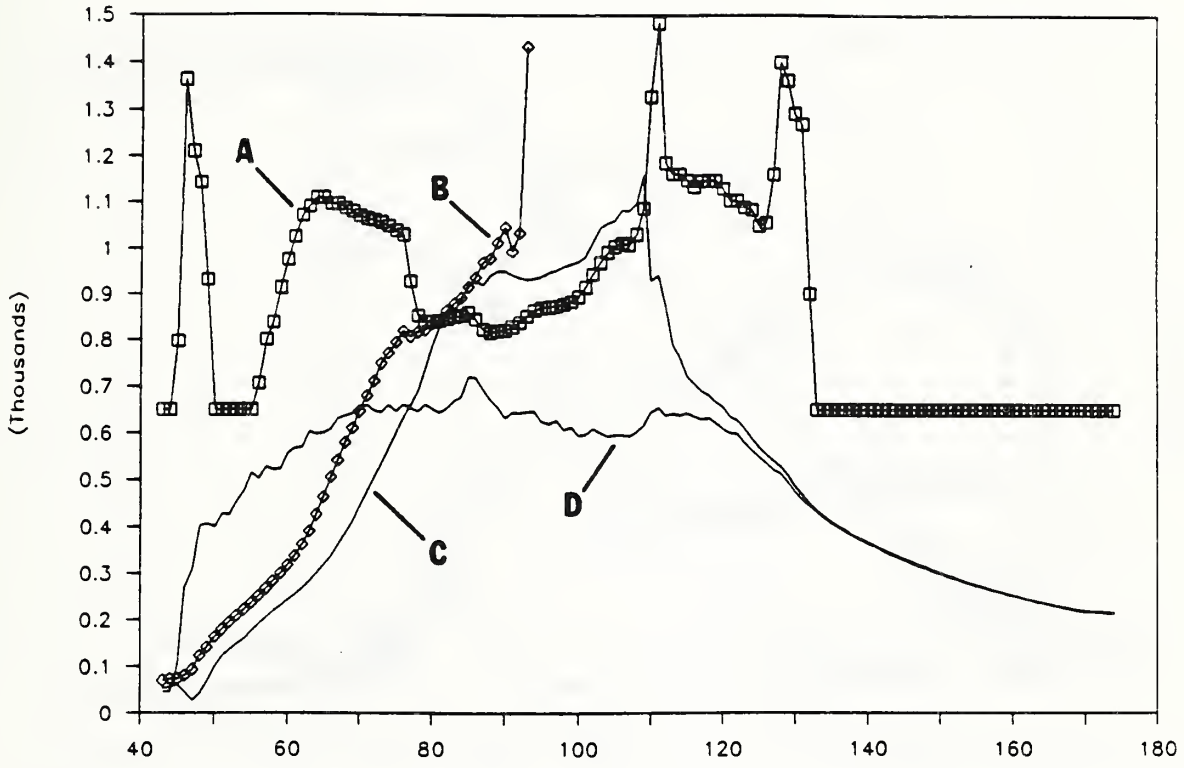

Figure 8 Sample Surface, Upper and Lower Internal Sample, and Gas Upper Side Temperatures versus Time
Experiment 112 (3.5% lime, 0.0% MnO_2)
Y axis: Temperature, °C, ; X axis: Arbitrary Time, minutes
A, Pyrometer temperature; B, Upper pellet thermocouple;
C, Lower pellet thermocouple; and D, Gas upper side thermocouple.

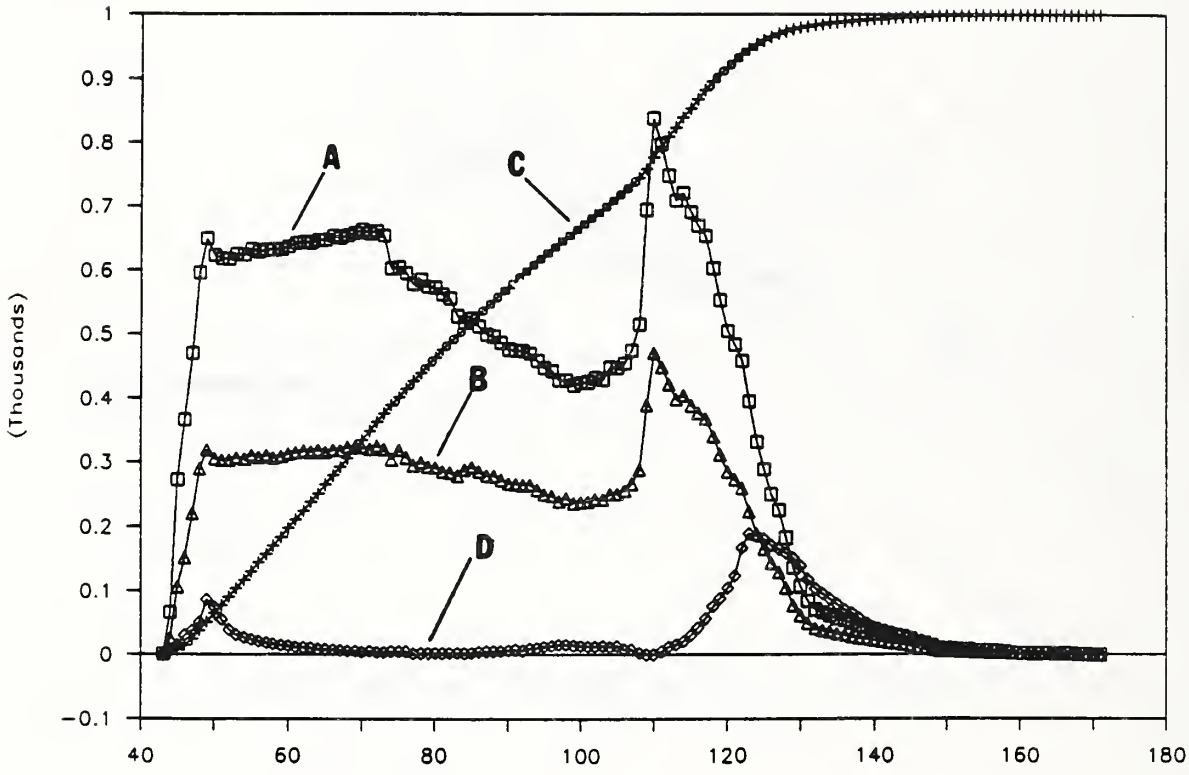

Figure 9 CO_2 and CO Production Rates, Oxygen Consumed/In, Fraction Reacted versus Time
Experiment 112 (3.5% lime, 0.0% MnO_2)
Y axis: arbitrary units, thousands; X axis: Arbitrary Time, minutes
A, CO_2 production, slpm x 20; B, O_2 consumed/O_2 in x 1000;
C, Fraction reacted x 1000; and D, CO production, slpm x 400.

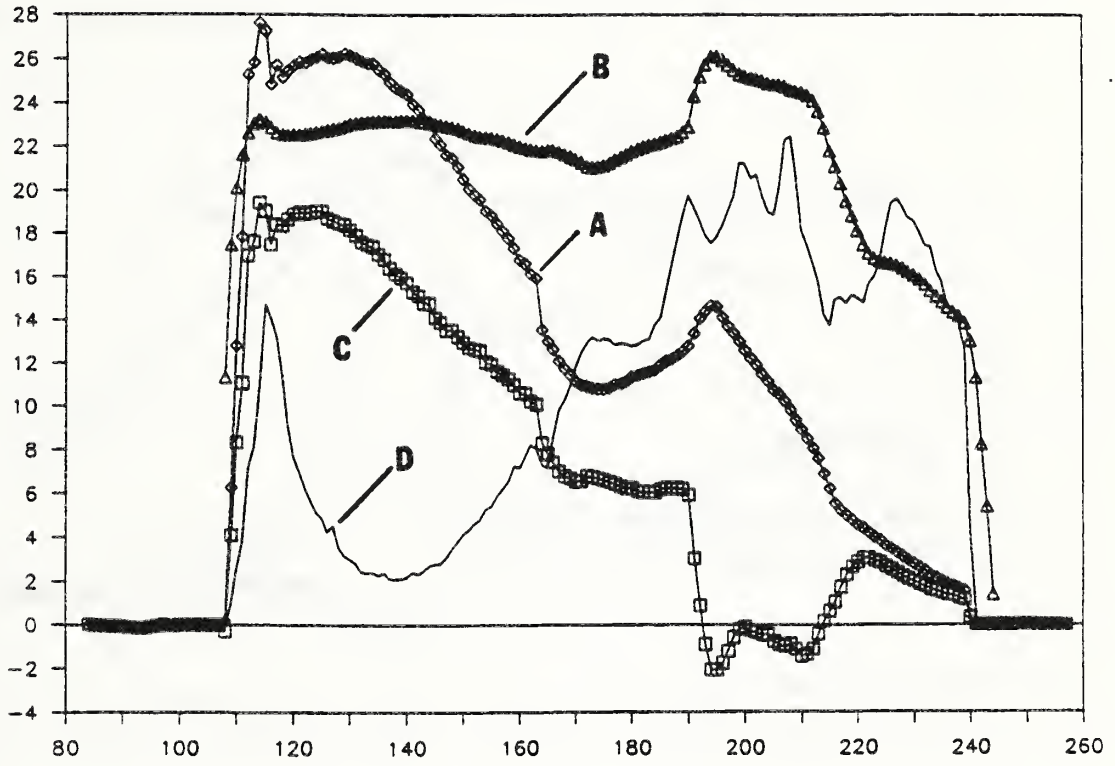

Figure 10 Sulfur Dioxide Capture
SO_2 Capture, Ash Temperature, and CO_2 and CO
Production Rates versus Time
Experiment 110 (7.1% lime, 0.2% MnO_2)
Y axis: arbitrary units, thousands; X axis: Arbitrary Time, minutes
A, CO_2 production, slpm; B, Reduced temperature of ash, $(T_{eq} - 1000K)/10K$, T_{eq} from equation (2); C, SO_2 capture: SO_2in - SO_2out, slpm x 100; and D, CO production, slpm x 100.

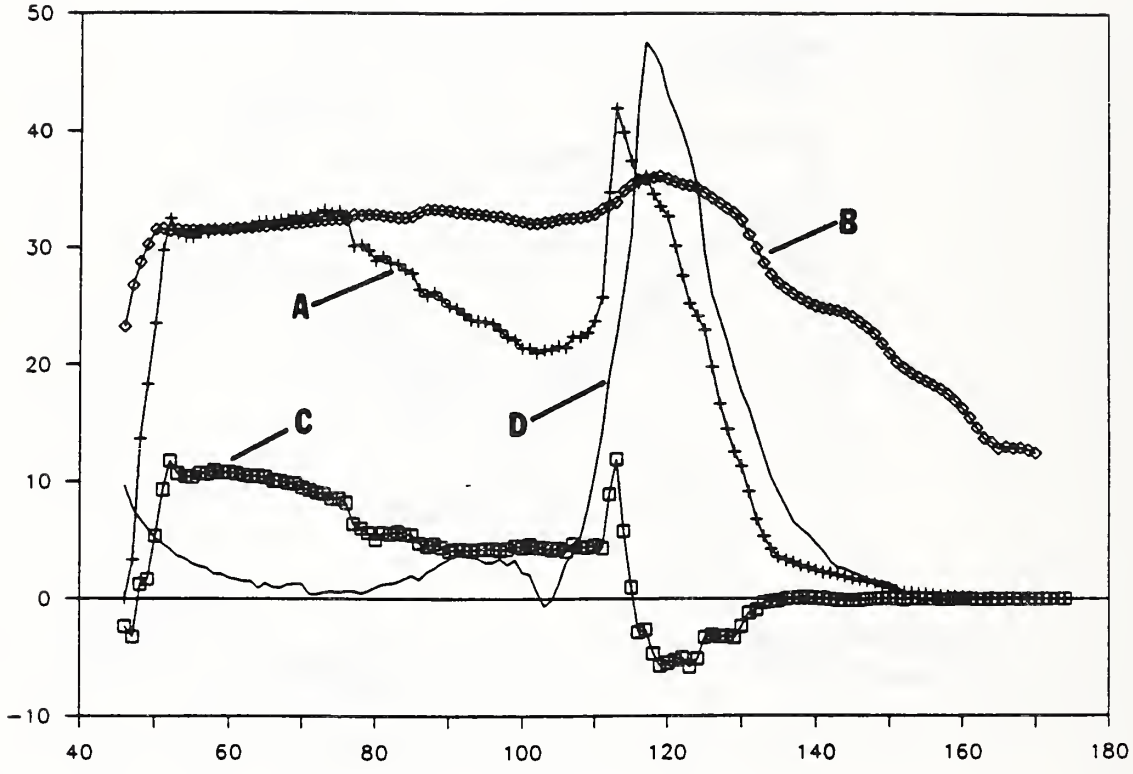

Figure 11 Sulfur Dioxide Capture
SO_2 Capture, Ash Temperature, and CO_2 and CO
Production Rates versus Time
Experiment 112 (3.5% lime, 0.0% MnO_2)
Y axis: arbitrary units, thousands; X axis: Arbitrary Time, minutes
A, CO_2 production, slpm; B, Reduced temperature of ash, $(T_{eq}$ - 1000K)/10K, T_{eq} from equation (2); C, SO_2 capture: SO_2in - SO_2out, slpm x 100; and D, CO production, slpm x 100.

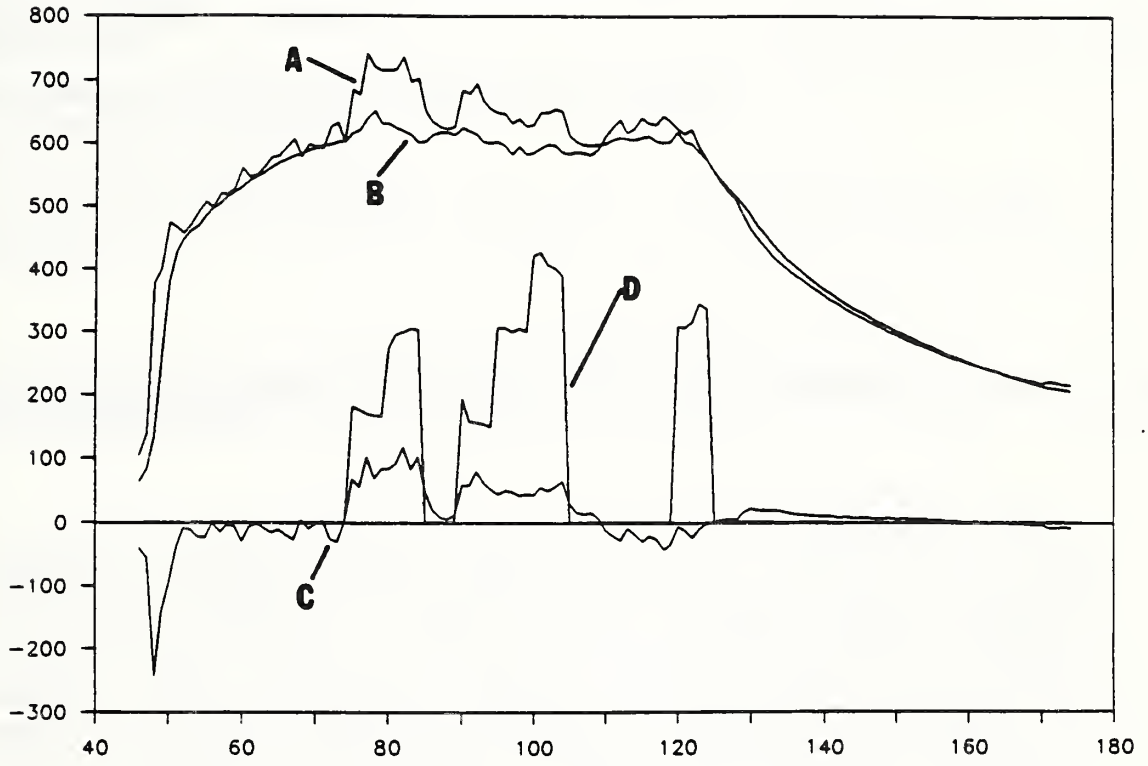

Figure 12 Aspiration Experiment Results
Experiment 112 (3.5% lime, 0.0% MnO_2)
Y axis: Temperature, °C, or Flow rate, slpm x 10;
X axis: Arbitrary Time, minutes
A, Aspirated gas lower side thermocouple, °C; B, Regular gas lower side thermocouple, °C; C, Aspirated minus regular gas lower side thermocouple, °C;
and D, Aspiration flow rate, slpm x 10.

NIST-114A
(REV. 3-89)

U.S. DEPARTMENT OF COMMERCE
NATIONAL INSTITUTE OF STANDARDS AND TECHNOLOGY

BIBLIOGRAPHIC DATA SHEET

1. PUBLICATION OR REPORT NUMBER
NISTIR 4443

2. PERFORMING ORGANIZATION REPORT NUMBER

3. PUBLICATION DATE
NOVEMBER 1990

4. TITLE AND SUBTITLE

SULFUR DIOXIDE CAPTURE IN THE COMBUSTION OF MIXTURES OF LIME, REFUSE-DERIVED FUEL, AND COAL

5. AUTHOR(S)

K.L. Churney and T.J. Buckley

6. PERFORMING ORGANIZATION (IF JOINT OR OTHER THAN NIST, SEE INSTRUCTIONS)

U.S. DEPARTMENT OF COMMERCE
NATIONAL INSTITUTE OF STANDARDS AND TECHNOLOGY
GAITHERSBURG, MD 20899

7. CONTRACT/GRANT NUMBER

8. TYPE OF REPORT AND PERIOD COVERED

9. SPONSORING ORGANIZATION NAME AND COMPLETE ADDRESS (STREET, CITY, STATE, ZIP)

U.S. Department of Commerce
Center for Chemical Technology
Chemical Thermodynamics Division
National Institute of Standards and Technology Gaithersburg, MD 20899

10. SUPPLEMENTARY NOTES

[ ] DOCUMENT DESCRIBES A COMPUTER PROGRAM; SF-185, FIPS SOFTWARE SUMMARY, IS ATTACHED.

11. ABSTRACT (A 200-WORD OR LESS FACTUAL SUMMARY OF MOST SIGNIFICANT INFORMATION. IF DOCUMENT INCLUDES A SIGNIFICANT BIBLIOGRAPHY OR LITERATURE SURVEY, MENTION IT HERE.)

Chlorine and sulfur mass balance studies have been carried out in the combustion of mixtures of lime, refuse-derived fuel, and coal in the NIST multikilogram capacity batch combustor. The catalytic effect of manganese dioxide on the trapping of sulfur dioxide by lime was examined. Under our conditions, only 4% of the chlorine was trapped in the ash and no effect of manganese dioxide was observed. Between 42 and 14% of the total sulfur was trapped in the ash, depending upon the lime concentration. The effect of manganese dioxide on sulfur capture was not detectable. The temperature of the ash was estimated to be near 1200 °C, which was in agreement with that calculated from sulfur dioxide capture thermodynamics.

12. KEY WORDS (6 TO 12 ENTRIES; ALPHABETICAL ORDER; CAPITALIZE ONLY PROPER NAMES; AND SEPARATE KEY WORDS BY SEMICOLONS)

ash; chlorine; coal; combustion; lime;manganese dioxide; refuse derived fuel

13. AVAILABILITY

[X] UNLIMITED

[ ] FOR OFFICIAL DISTRIBUTION. DO NOT RELEASE TO NATIONAL TECHNICAL INFORMATION SERVICE (NTIS).

[ ] ORDER FROM SUPERINTENDENT OF DOCUMENTS, U.S. GOVERNMENT PRINTING OFFICE, WASHINGTON, DC 20402.

[X] ORDER FROM NATIONAL TECHNICAL INFORMATION SERVICE (NTIS), SPRINGFIELD, VA 22161.

14. NUMBER OF PRINTED PAGES
58

15. PRICE
A04

ELECTRONIC FORM